Available online at www.sciencedirect.com
ScienceDirect
Geochimica et Cosmochimica Acta 74 (2010) 1201–1219
Geochimica et Cosmochimica Acta
www.elsevier.com/locate/gca

Multicomponent diffusion of a suite of tracers (HTO, Cl, Br, I, Na, Sr, Cs) in a single sample of Opalinus Clay

C.A.J. Appelo [a,*], L.R. Van Loon [b], P. Wersin [c]

[a] Hydrochemical Consultant, Valeriusstraat 11, 1071 MB Amsterdam, The Netherlands
[b] Laboratory for Waste Management, Paul Scherrer Institut, CH-5232 Villigen PSI, Switzerland
[c] Gruner AG. Ingenieure und Planer, Gellertstrasse 55, CH-4020 Basel, Switzerland

Received 3 April 2009; accepted in revised form 9 November 2009; available online 17 November 2009

Abstract

Diffusion experiments with HTO, $^{36}Cl^-$, Br^-, I^-, $^{22}Na^+$, $^{85}Sr^{2+}$ and $^{134}Cs^+$ at trace concentrations in a single sample of Opalinus Clay are modeled with PHREEQC's multicomponent diffusion module. The model is used first in a classical approach to derive accessible porosities, geometrical factors (the ratio of pore tortuosity and constrictivity) and sorption behavior of the individual tracers assuming that the clay is homogeneous. The accessible porosity for neutral species and cations is obtained from HTO, the anion exclusion volume from $^{36}Cl^-$ and Br^-, and the cation exchange capacity from $^{22}Na^+$. The homogeneous model works well for tritium, the anions and $^{22}Na^+$. However, the $^{85}Sr^{2+}$ and $^{134}Cs^+$ experiments show an early arrival of the tracer and a front-form that suggest a dual porosity structure. A model with 10% dead-end pores, containing 19% of the total exchange capacity, can satisfactorily calculate all the experimental data. The Cs^+ diffusion model builds on a 3-site exchange model, constructed from batch sorption data. The excellent agreement of modeled and measured data contradicts earlier reports that the exchange capacity for Cs^+ would be smaller in diffusion than in batch experiments.

The geometrical factors for the anions are 1.5 times larger than for HTO, and for the cations 2–4 times smaller than for HTO. The different behavior is explained by a tripartite division of the porespace in free porewater, diffuse double layer (DDL) water, and interlayer water in montmorillonite. Differences between estimated and observed geometrical factors for cations are attributed to increased ion-pairing of the divalent cations in DDL water as a result of the low relative dielectric permittivity. Interlayer and/or surface diffusion contributes significantly to the diffusive flux of Cs^+ but is negligible for the other solutes. The geometrical factors for anions are higher than estimated, because pore constrictions with overlapping double layers force the anions to take longer routes than HTO and the cations. Small differences among the anions can also be attributed to different ion-pairing in DDL water.

1. INTRODUCTION

Opalinus Clay (OPA) is a geological formation in the northern part of Switzerland with suitable properties for hosting a repository for high-level radioactive waste (Nagra, 2002a). The virgin rock has a very low hydraulic conductivity, ranging from 10^{-14} to 10^{-12} m/s (Croisé et al., 2004), and diffusion is therefore the main transport mechanism for radionuclides released from a repository. Several diffusion studies have been performed to obtain transport parameters for OPA, both in the laboratory under well-defined conditions (Van Loon et al., 2003a, 2004a, 2005), and in the field under more realistic *in-situ* settings (Palut et al., 2003; Van Loon et al., 2004b; Wersin et al., 2004, 2007). The field experiments were done in the Underground Research Laboratory (URL) at Mont Terri (Thury and Bossart, 1999).

The experiments provide apparent diffusion coefficients for the tracers, which are a function of the solute's tracer diffusion coefficient in water, the geometrical factor that

* Corresponding author. Tel.: +31 206716366.
E-mail address: appt@xs4all.nl (C.A.J. Appelo).

0016-7037/$ - see front matter © 2009 Elsevier Ltd. All rights reserved.
doi:10.1016/j.gca.2009.11.013

accounts for the tortuous and occasionally constricted path in the clay, the accessible porosity, and the distribution coefficient that is regulated by the affinity for sorption sites. The diffusion and distribution coefficients are well known to be different for various solutes (Boudreau, 1997; Appelo and Postma, 2005). Perhaps more surprising, and anyhow less well understood, is that also the accessible porosity and the geometrical factor are different for the various tracers. In Opalinus Clay, diffusion of cations is enhanced, and that of anions diminished, relative to a neutral tracer such as tritiated water (HTO). This is in line with results from many other diffusion experiments with clayrock, bentonite or pure montmorillonite (Shackelford and Daniel, 1991; Sato et al., 1992; Sato, 2005; Kozaki et al., 1998, 2005, 2008; Molera and Eriksen, 2002; Van Loon et al., 2003a,b; 2004a,b; 2007; Melkior et al., 2007; Wersin et al., 2007; Descostes et al., 2008). The increased diffusion of cations is explained either by interlayer or surface diffusion of sorbed cations (Ohlsson and Neretnieks, 1998; Eriksen et al., 1999; Bourg, 2004; Bourg et al., 2007; Glaus et al., 2007), or by diffusion in the diffuse double layer (DDL) that surrounds the negatively charged clay surface and contains an excess of cations (Van Schaik et al., 1966; Kemper and Quirk, 1972; Ochs et al., 1998, 2001; Lehikoinen et al., 1999; Leroy and Revil, 2004; Leroy et al., 2006; Appelo and Wersin, 2007; Jougnot et al., 2009).

The concepts that are invoked to explain the different diffusion behavior are illustrated in a sketch of the porespace in Opalinus Clay in Fig. 1 (NAGRA, 2002b; Bradbury and Baeyens, 2003; Appelo et al., 2008). The largest pores contain free porewater, an electrically neutral solution. Close to the surface of the clay, the free porewater becomes charged by an excess of counter-ions and a deficit of co-ions and turns into a diffuse double layer (DDL). At the surface *per se*, exchangeable cations form complexes with surface oxygens. Interlayer water in montmorillonite is the third type, and assumed to contain exchangeable cations only which behave chemically and physically comparable to the surface complexed cations. Diffusion in free porewater is similar to diffusion in pure water, but the flux is less because the tortuous path in the pores is longer than the straight-line distance used for defining the concentration gradient in Fick's laws. The excess of cations in the DDL gives an increase of the concentration gradient in the free (uncharged) pores and thus, diffusion of cations is enhanced (Van Schaik et al., 1966; Kemper and Quirk, 1972; Ochs et al., 1998, 2001; Lehikoinen et al., 1999; Leroy and Revil, 2004; Leroy et al., 2006; Appelo and Wersin, 2007; Jougnot et al., 2009). Also, the deficit of anions in the DDL explains why anions diffuse more slowly (Lehikoinen et al., 1999; Ochs et al., 2001; Leroy et al., 2006; Jougnot et al., 2009), and why the accessible porosity is smaller for anions than for cations (Bolt and De Haan, 1982; Muurinen et al., 2004, 2007; Van Loon et al., 2007).

Another enigma is the apparent mismatch of distribution coefficients for Cs^+ in diffusion and batch experiments using the same material. To model Cs-data from the field experiments, both Van Loon et al. (2004b) and Wersin et al. (2007) used a Freundlich-type isotherm with a twice smaller sorption capacity than found in batch experiments by Lauber et al. (2000). While modeling another diffusion experiment with tabulated slopes for the same sorption isotherm, Jakob et al. (2009) reduced the sorption capacity for Cs^+ even five times. Maes et al. (2008) also invoked a smaller sorption capacity for diffusion of Cs^+ in Boom clay than found in batch experiments. One difficulty, not fully recognized so far, is that the very strong partitioning of Cs^+ towards the solid phase leaves less than 1% of the total mass in solution. Modeling of transport requires then a very accurate incorporation of the details of the (non-linear) sorption isotherm. In addition, field experiments in OPA show a highly irregular distribution of diffused tracer Cs^+ in the rock, which is linked to spatial variations of the illite content (Grolimund et al., 2005). This indicates that some pores are lined with surfaces that sorb Cs^+ very strongly and remove Cs^+ almost completely from solution until the sorption sites are filled. If these pores are dead-ended, the concentration of Cs^+ may be kept at a low level that cannot be resupplied sufficiently quickly from more continuous pores during the passage of a front. As a result of this

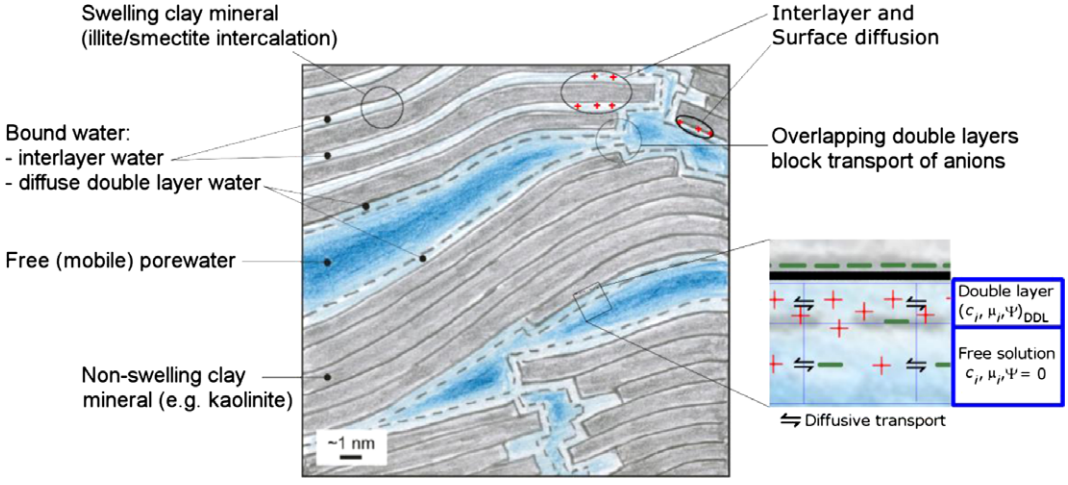

Fig. 1. A diagram of the porespace in Opalinus Clay, showing three water-types with associated diffusion domains (modified from NAGRA, 2002b). Right hand side: representation of a pore in PHREEQC.

physical non-equilibrium, the front travels more rapidly than when all the pores and sorption sites react instantaneously. In the model-studies noted above, this was counterbalanced by reducing the sorption capacity for Cs^+. However, as will be shown in this paper, the sorption isotherm of Cs^+ from batch experiments is valid in diffusive transport as well when dead-end pores are accounted for.

In order to develop a consistent model that encompasses the diffusion of all the tracers together, the data of Van Loon et al. (2004a) were remodeled together with new measurements of I^-, Br^-, $^{85}Sr^{2+}$ and $^{134}Cs^+$. Van Loon et al. (2003a,b; 2004a,b; 2005) and Wersin et al. (2004, 2007) used a single porosity medium with a homogeneous distribution of the surface charge, and ignored the effect of the filters that enclose the sample. The model presented here introduces a dual porosity structure with dead-end pores for diffusion, assumes a heterogeneous distribution of surface charge over the porosity domains, and takes the filters into account. The model was implemented in PHREEQC (Parkhurst and Appelo, 1999) and makes use of the multicomponent diffusion module of Appelo and Wersin (2007). Following the modeling, it will be investigated how the different geometrical factors for the seven tracers are related to porespace properties when subdivided as in Fig. 1, viz. in free porewater, DDL water, and interlayer water.

2. MATERIALS, METHODS AND MODEL STRUCTURE

2.1. Mineralogy/water chemistry

The OPA sample used in the diffusion experiments originates from the Mont Terri URL and was taken in the gallery used for the *in-situ* experiments (Van Loon et al., 2004b; Wersin et al., 2007). The mineralogical composition of the specific sample was not analyzed, but the properties of the clayrock close-by are presented in Table 1. The synthetic OPA porewater composition for the Mont Terri OPA system was prepared according to Pearson (1998) and is given in Table 2. The water contains oxygen and is in equilibrium with the laboratory's atmosphere.

Table 1
Mineralogy and other properties of Opalinus clay from Mont Terri (Nagra, 2002b). The cation exchange capacity (*CEC*) was determined from the diffusion experiment with ^{22}Na (stagnant model).

Minerals	Mont Terri OPA (wt.%)
Calcite	13 ± 8
Dolomite/ankerite	n.d.[a]
Siderite	3.0 ± 1.8
Quartz	14 ± 4
Albite	1 ± 1.0
K-Feldspar	1 ± 1.6
Pyrite	1.1 ± 0.5
Total phyllosilicates	66 ± 11
Illite	23 ± 2
Illite/smectite mixed layer	11 ± 2
Kaolinite	22 ± 2
Chlorite	10 ± 2
Organic carbon	0.8 ± 0.5
CEC/(meq/kg dry)	124
Dry density/(kg/L)	2.7

[a] n.d.: not detectable.

2.2. Radial diffusion experiment

The sample preparation, the experimental set-up and the theory of the radial through-diffusion method is described in detail in Van Loon et al. (2004a). A cylindrical sample was prepared with the axis normal to the bedding plane of the clay. The inner and outer radius of the sample was 6.58 and 25.4 mm, respectively, and the height was 52 mm. The sample was introduced in the diffusion cell between cylindrical stainless steel filters with thicknesses of 1.6 and 1.8 mm for the inner and outer one, respectively. End plates were mounted at the top and bottom of the sample and pressurized to 7 MPa, which represents the burden load on the Opalinus Clay formation in Mont Terri. The sample was resaturated with artificial pore water (see Table 2) for 1 month. Hereafter, the diffusion experiments were started. The experiments were continued until diffusion through the sample reached steady state, except for Cs^+, which is sorbed too strongly. All experiments were performed at a temperature of 23 ± 2 °C. The timeframe is listed in electronic annex EA-1.

2.3. Batch experiments for Cs^+ sorption

Sorption of Cs^+ was measured on crushed and intact samples from the same core of Opalinus Clay that was used in the diffusion experiments following procedures described by Lauber et al. (2000). A detailed description of the sorption measurements is given in Van Loon et al. (2009).

2.4. Tracers and tracer analysis

The procedures for the tracers HTO, $^{36}Cl^-$ and $^{22}Na^+$ have been described by Van Loon et al. (2004a). Following those experiments, stable I^- and Br^- tracers were added in form of NaI and NaBr to the artificial pore water. The concentration in the source reservoir was 10^{-3} M and had no effect on the ionic strength of the pore water. The amount of diffused I^- and Br^- in the receiving reservoir was measured by High Performance Liquid Chromatography (Dionex, DX-600) using an Ionpac AS16 4×250 mm analytical anion exchange column equipped with an Ionpac AG16 4×50 mm guard column. The eluent was 40 mM NaOH. The eluted ions were detected by electric conductivity measurements and reducing the background conductivity with a self-regenerating suppressor (ASRS). The detection limit for I^- and Br^- analysis was 5×10^{-6} M.

$^{85}Sr^{2+}$ and $^{134}Cs^+$ were purchased from Isotope Products Europe (Germany). The activity concentration of the tracers in the source reservoir was 1000 Bq/cm^3. The background concentrations of stable Sr^{2+} and Cs^+ were 5.1×10^{-4} M (see Table 2) and 1.0×10^{-3} M, respectively. ^{134}Cs was measured by γ-counting (Minaxi-γ, Autogamma 5000 series, Packard) and ^{85}Sr by liquid scintillation counting (Tri-Carb 2250 CA, Canberra-Packard) using Ultima Gold XR (Canberra-Packard) as scintillation cocktail.

Table 2
Concentrations (mmol/L, except pH) in the boundary fluids, diffusion coefficients and surface complexation constants (log K_{iSu}) in the model. The free water diffusion coefficients (D_w) are for 25 °C (Boudreau, 1997). Log K_{NaSu} is fixed, other log K_{iSu}'s were adapted to make the sum of surface and DDL concentrations equal with the exchangeable cation concentrations according to Pearson et al. (2003); log K_{SrSu2} is determined in the experiment with ^{85}Sr (stagnant model).

	Concentration	D_w (10^{-9} m^2/s)	log K	
pH	7.6	9.31	2.3	(H^+)
Na^+	240	1.33	−0.7	
K^+	1.61	1.96	0.15	
Mg^{2+}	16.9	0.705	−0.56	
Ca^{2+}	25.8	0.793	−0.32	
Sr^{2+}	0.505	0.794	0.20	
Cl^-	300	2.03		
Alkalinity	0.476	1.18		(HCO_3^-)
SO_4^{2-}	14.1	1.07		
OH^-		5.27		

The measured activities were corrected for radioactive decay. The detection limits for the activity measurements was ca. 1 Bq.

2.5. Uncertainty estimations

The uncertainty in the values of the fluxes and the accumulated diffused mass in the through-diffusion measurements results mainly from random variations in the count rates and the counting efficiency, the dead volumes in the diffusion cell and the tubings and filters, and errors in the pipetting and weighing procedures. Details for estimating the overall uncertainty are given in Van Loon and Soler (2004). The uncertainty in the precision of the flux is estimated to be about 10% (Van Loon et al., 2004a). The accuracy probably varies for the tracers, but the standard deviation in the diffusion coefficient calculated from the data is (much) smaller than 10% for all (cf. Table 3).

2.6. Model structure and configuration

The experimental data were fitted with a diffusive transport model to obtain the parameters in Fick's diffusion equations for the overall pore. The diffusional flux of species i is:

$$J_i = -\frac{u_i c_i}{|z_i|F}\frac{\partial \mu_i}{\partial x} \quad (1)$$

where J_i is the flux (mol/m^2/s), u_i is the mobility (m^2/s/V), c_i is the concentration (mol/m^3), z_i is charge number (−), F is the Faraday constant (96485J/V/eq), x is distance (m), and μ_i is the thermodynamic potential, given by:

$$\mu_i = \mu_i^0 + RT\ln[i] + z_i F\psi \quad (2)$$

where μ_i^0 is the standard potential (J/mol), R is the gas constant (8.314 J/K/mol), T is the absolute temperature (K), $[i]$ is the activity (−), and ψ is the electric potential (V). The activity in water is related to concentration by $[i] = \gamma_i\, c_i/(1000c^0)$, where γ_i is the activity coefficient (−) and c^0 is the standard state (1 mol/kg H_2O, taken equal to 1 mol/L in the following).

Assuming an activity coefficient $\gamma_i = 1$ and an electric potential gradient $\partial\psi/\partial x = 0$, and using the identities $u_i = D_{w,i}\,|z_i|\,F\,/\,(RT)$ and $c\ \mathrm{d}(\ln c) = \mathrm{d}(c)$, Eq. (1) becomes Fick's law:

$$J_i = -D_{w,i}\frac{\mathrm{d}c_i}{\mathrm{d}x} \quad (3)$$

where $D_{w,i}$ is the diffusion coefficient in water (m^2/s).

In a porous medium, the porewater diffusion coefficient ($D_{p,i}$) differs from the diffusion coefficient in free water by

Table 3
Accessible porosities (ε_a), geometrical factors (G) and distribution coefficients (K_d/(mol/L/mol/L)) for tritium (HTO), Cl^-, Br^-, I^-, Na^+, Sr^{2+} and Cs^+. Numbers with standard deviation indicated are optimized; numbers without are taken from experiments with another solute, except G for Cs^+ (see text).

	Homogeneous			With dead-end pores		
	ε_a	G	K_d	ε_a	G	K_d
HTO(1)	0.162 ± 0.001	6.33 ± 0.05	0	0.167 ± 0.001	5.87 ± 0.07	0
HTO(2)	0.155 ± 0.003	5.96 ± 0.19	0	0.156 ± 0.003	5.43 ± 0.20	0
Average	0.159	6.14	0	0.161	5.65	0
$^{36}Cl^-$	0.077 ± 0.001	9.24 ± 0.13	0	0.078 ± 0.001	8.47 ± 0.13	0
Br^-	0.078 ± 0.002	9.54 ± 0.22	0	0.085 ± 0.001	9.36 ± 0.17	0
I^-	0.105 ± 0.003	14.5 ± 0.8	0	0.076 ± 0.006	9.8 ± 0.7	0
I^-	0.077	10.7 ± 0.05	0.029 ± 0.003	0.081	10.04 ± 0.05	0.021 ± 0.003
$^{22}Na^+$	0.159	2.21 ± 0.00	3.41 ± 0.03	0.161	2.16 ± 0.00	3.58 ± 0.04
$^{85}Sr^{2+}$	0.159	1.68 ± 0.00	24.3 ± 0.2	0.161	1.44 ± 0.00	26.3 ± 0.2
$^{134}Cs^+$	0.159		Variable	0.161	1.44	Variable

tortuosity and constrictivity factors (Dullien, 1992; Van Brakel and Heertjes, 1974):

$$D_{p,i} = \frac{\delta}{\theta^2} D_{w,i} \tag{4}$$

The tortuosity factor (θ^2) expresses that diffusing molecules have to pass around solid grains and take a longer path (L_a) than the straight-line distance (L). A tortuous path at an angle of 45° with the straight-line distance obviously gives a tortuosity $\theta = 2/\sqrt{2} = 1.4$, and a tortuosity factor $\theta^2 = 2$. The constrictivity factor (δ) encompasses effects of pore narrowing and widening. A straight pore has a constrictivity factor of 1, if the pore narrows it becomes smaller than 1, and if it widens, larger than 1. Inert porous media have constrictivity factors slightly smaller than 1 (Van Brakel and Heertjes, 1974).

Since it is difficult to discern tortuosity and constrictivity for a natural porous medium, the two are conveniently assembled in the geometrical factor (G_i), which is related by Archie's law to the accessible porosity ($\varepsilon_{a,i}$) (Grathwohl, 1998; Van Loon et al., 2007):

$$\frac{\delta}{\theta^2} = \frac{1}{G_i} = (\varepsilon_{a,i})^n \tag{5}$$

where n is an empirical factor (≈1).

In the flux equation, diffusion is calculated for the surface area that is accessible for the solute. The steady state flux in the porous medium becomes:

$$J_i = -\varepsilon_{a,i} \frac{D_{w,i}}{G_i} \frac{\mathrm{d}c_i}{\mathrm{d}x} = -D_{e,i} \frac{\mathrm{d}c_i}{\mathrm{d}x} \tag{6}$$

where $D_{e,i}$ is the effective diffusion coefficient (m^2/s).

Before steady state is reached, the concentration changes in the radial field ($x = r$) of the experiment are given by:

$$\frac{\partial}{\partial t}\left(c_i + s_i \frac{\rho_b}{\varepsilon_{a,i}}\right) = D_{p,i}\left(\frac{\partial^2 c_i}{\partial r^2} + \frac{1}{r}\frac{\partial c}{\partial r}\right) \tag{7}$$

where t is time (s), s_i is the concentration in the solid (mol/kg), and ρ_b is the solid's bulk density (kg/m^3).

The radial diffusion field in the experiment was modeled with PHREEQC, using explicit, second order accurate finite differences (Appelo et al., 2008; a c-program that writes the PHREEQC input file for Cs^+ diffusion is listed in EA-1). The harmonic mean of the accessible porosity and the geometrical factor were used for calculating the flux over the interface between 2 cells:

$$J_{12,i} = -\frac{2\frac{\varepsilon_{a1,i}}{G_{1,i}}\frac{\varepsilon_{a2,i}}{G_{2,i}}}{\Delta r_2 \frac{\varepsilon_{a1,i}}{G_{1,i}} + \Delta r_1 \frac{\varepsilon_{a2,i}}{G_{2,i}}} D_{w,i}(c_{2,i} - c_{1,i}) \tag{8}$$

where J_{12} is the flux between cells 1 and 2, subscripts 1 and 2 indicate the cell, and Δr is the cell length (m).

Fig. 2 shows the outline of the model grid with dead-end pores. Cell-numbers are indicated in red in Fig. 2. The numbering determines the computation order for PHREEQC and should follow the major transport routes. The geometrical factor of the filters (colored grey) was fixed to $G = 10$ for all the tracers, as measured by Glaus et al. (2008). The porosity of the filters was 0.418 and 0.367 for the inner and outer filter, respectively. For the sample, the accessible porosity, the geometrical factor and the sorption properties were optimized with the non-linear, least squares code PEST (Doherty, 1994). The model accuracy was checked by varying the time step, *nr* and *nz* and the number of cells used for the filters. The results reported here were obtained with $nr = 13$, with 1 cell used for each filter and 11 for the sample.

2.7. Surface complexation model for cation exchange

Cation exchange between water and clay was calculated by combining Dzombak and Morel's (1990) surface complexation model and the Donnan approximation of the diffuse double layer (Appelo and Wersin, 2007). The surface complexation reactions are, for example for Na^+ and Ca^{2+} on surface sites Su^-:

$$Na^+ + Su^- \leftrightarrow NaSu; \quad \log K_{NaSu} = -0.7 \tag{9}$$

$$Ca^{2+} + 2Su^- \leftrightarrow CaSu_2; \quad \log K_{CaSu_2} = 2\log K_{NaSu} + 1.08 = -0.32 \tag{10}$$

Subtracting Equation (9) twice from Eq. (10) gives the traditional equation for Na^+–Ca^{2+} exchange.

Not all the surface sites are occupied by cations. The charge of the empty sites is compensated by the diffuse double layer, approximated by a Donnan volume in which the concentrations are related with Boltzmann's equation to the concentrations in free porewater:

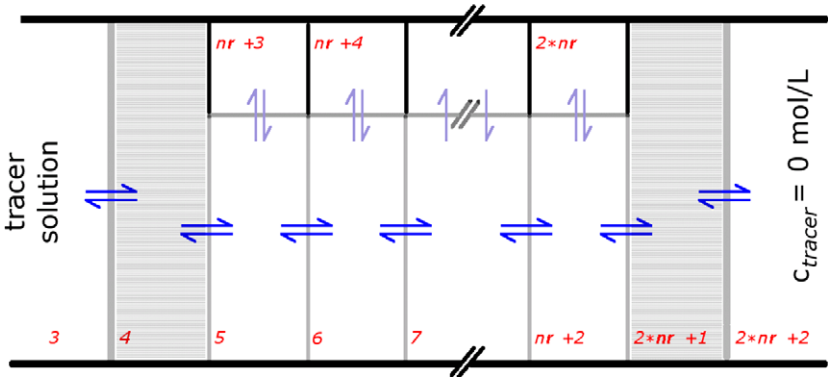

Fig. 2. Outline of the radial grid in the PHREEQC model with dead-end pores. The filter-cells are indicated in grey.

$$c_{\mathrm{DDL},i} = c_{free,i}\exp\left(\frac{-z_i F\psi_D}{RT}\right) \quad (11)$$

where $c_{\mathrm{DDL},i}$ is concentration of i in the Donnan volume (mol/kg water, assumed equal to mol/L), c_{free} is the concentration in free porewater, z is the charge number, F is the Faraday constant (96485 J/V/eq), ψ_D the potential in the Donnan volume (V), R the gas constant (8.314 J/K/mol) and T the temperature (K).

The potential ψ_D is defined by letting the charge of the Donnan volume counterbalance the net-charge of the surface (not complexed by cations):

$$\Sigma(\mathrm{kgH_2O})_{\mathrm{DDL}} \times zic_{\mathrm{DDL}}, i + eq_S u = 0 \quad (12)$$

where $(\mathrm{kg\ H_2O})_{\mathrm{DDL}}$ is the mass of water in the Donnan volume and eq_{Su} is the charge of the surface (eq).

The partitioning of the total surface charge over the DDL and the surface sites affects the distribution coefficient (s_i/c_i) because the ratios of the ions are different in the surface sites and in the DDL. In turn, this has a bearing on the surface potential and on complexation (Dzombak and Hudson, 1995). According to the Boltzmann equation, the ratios of equal-charged cations are the same in the DDL and the solution. In the surface sites, the ratios mainly depend on the chemical selectivity given by the surface complexation constant. If the surface complexation constants are higher than 10^{10}, all the surface sites are occupied by cations and the DDL-charge is zero. If, on the other hand, the constants are smaller than 10^{-10}, the surface sites are empty and the surface charge is compensated in the DDL. At intermediate values the charge is distributed over the two domains, depending also on the composition of the solution, the surface potential and the surface area. The reference log $K_{\mathrm{NaSu}} = -0.7$, the value adopted by Dzombak and Hudson (1995), Appelo and Wersin (2007) and Appelo et al. (2008).

Fig. 3 shows that the surface area also affects the distribution coefficients. If the surface area is large, the electrostatic contribution to surface complexation is negligible, resulting in 95% of the surface charge being compensated in the DDL. The distribution coefficients of Na^+ and K^+ are then nearly the same. If the surface area decreases, charge neutralization changes from DDL to surface sites. As a result, the distribution coefficients of Na^+ and K^+ diverge by a factor of 7, the constant for K^+/Na^+ exchange. The trend in the distribution coefficients of Mg^{2+} and Ca^{2+} can be interpreted similarly and the behavior of groups of monovalent and divalent cations follow this pattern as well. In the model, the measured BET value of 37 m^2/g was adopted since it agrees with the average pore diameter of 8 nm found by mercury porosimetry (Gimmi, 2003; Pearson et al., 2003). It results in 45% of the surface charge being compensated in the DDL. Using this surface area, the values of the surface complexation constants for the major cations were adapted to give the distribution coefficients calculated from measured exchange constants for Opalinus Clay (Pearson et al., 2003; Fig. 3). The constants are listed in Table 2.

2.8. Modeling strategy

The experiments were run until the diffusional flux reached steady state, within the limits imposed by the available mass in the reservoir and the sorption capacity of the clay. The steady state flux provides the effective diffusion coefficient of the tracer (Eq. (6)), while the delay in the steady state arrival time gives the mass that is stored in the accessible porosity and the sum of sorption sites and DDL (Eq. (7)). For extracting the geometrical factor from the effective diffusion coefficient, the accessible porosity is needed, but this parameter can be determined only for HTO and non-sorbing anions from diffusion experiments. For cations, also the cation

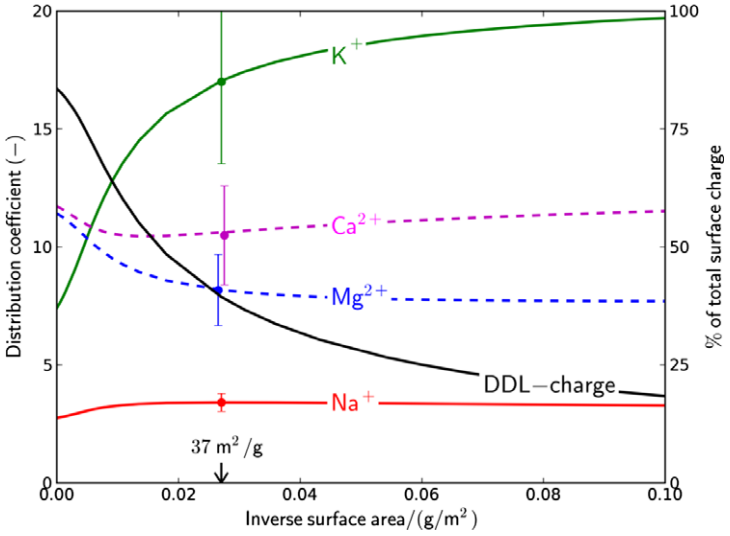

Fig. 3. Distribution coefficients (moles sorbed + DDL/moles solute) and DDL-charge calculated by the surface complexation model as a function of the (inverse) surface area. The DDL-charge is expressed as a percentage of the total surface charge. The average BET surface area of Opalinus Clay is 37 m^2/g. Data points with error bars are the distribution coefficients according to averaged cation exchange constants from Pearson et al. (2003), p. 224.

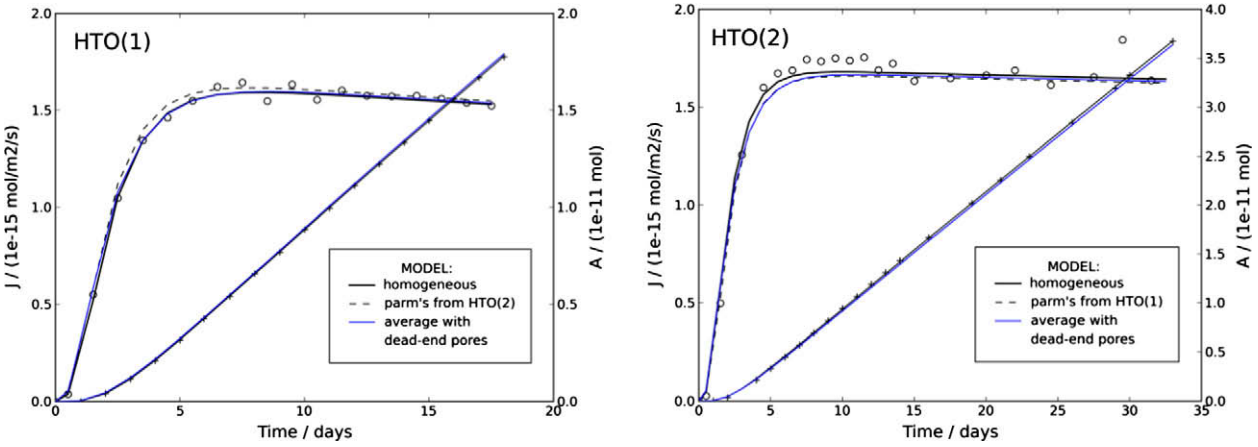

Fig. 4. Cumulative mass outflow (A, + symbols) and corresponding flux (J, o symbols) of HTO in two diffusion experiments and model lines for a homogeneous medium (solid lines if optimized for the experiment, dashed lines with the parameters from the companion experiment) and for a dual porosity medium with 10% dead-end pores, an overall porosity of 0.161 and averaged geometrical factor (blue lines). (For interpretation of the references to color in this figure legend, the reader is referred to the web version of this article.)

exchange capacity is a variable that must be resolved. The interdependency of the parameters necessitates a step-by-step approach, first modeling HTO to obtain the total porosity, and next, modeling the anions to find the anion-accessible porosity. The difference gives the amount of DDL water, which (optionally in PHREEQC) is assigned to be devoid of anions. Also with this option, the concentration gradient for calculating the diffusive flux of counter-ions in the DDL is set equal to the gradient in free pore water. By optimizing the model outcome on the measured, accumulated mass outflow of the tracers, it allows to obtain the effective diffusion coefficient of cations in the traditional manner together with parameters in the chemical model.

For Cs^+, a model with three surface sites of different strengths was constructed that fits the measured sorption isotherm, and the geometrical factor was adapted in the diffusion model. Comparison with the data indicated that diffusion of Cs^+ was affected by heterogeneities in the sample. A dual porosity structure, with the exchange capacity distributed differently over dead-end and continuous pores, showed the best results. This refined model with dead-end pores was run once again to obtain the variables for all the tracers together. This stage showed delicate interdependencies of the physical and chemical model parameters: the fraction of dead-end pores was limited for HTO, the anions, and Na^+, and thus, also for Cs^+, assuming that the physical properties of the sample remained the same over the 2.6 years that the experiment lasted.

3. RESULTS

Results of the homogeneous and dead-end pore models are presented in Figs. 4–7 for the tracers. For Cs^+ the effects of changing various parameters are shown in Fig. 9. The resulting geometrical factors are listed in Table 3.

3.1. Modeling HTO, $^{36}Cl^-$, Br^- and I^-

Two consecutive experiments with HTO are shown in Fig. 4. The volume of the tracer solution was 0.2 L for the experiment marked as HTO(1) and 1 L for HTO(2). The smaller reservoir used for HTO(1) was depleted more quickly which resulted in a more clearly declining flux after 10 days. The porosities and geometrical factors found for the two experiments can be compared, following the solid and dashed black lines which were calculated with the optimized numbers for the set, and with the numbers from the companion set, respectively. The small differences are within the uncertainty range of the two experiments (1% for HTO(1) and 4% for HTO(2)).

The blue lines are for the model with dead-end pores (adopted on the basis of the Sr^{2+} and Cs^+ experiments), with the geometrical factors averaged for the two HTO experiments. For an individual experiment, both the homogeneous and the dead-end pores model provide equal fit with the data if the geometrical factor is adapted. With the averaged values, the fit deteriorates somewhat for HTO(2), for which the flux-data points lie above the model lines during the transition stage to steady state. Probably, these details are insignificant in view of the experimental error.

For the anions, the experimental data and model lines are shown in Fig. 5. Again, the black lines stem from the homogeneous model in which the accessible porosity and the geometrical factor are optimized. The blue lines represent the fit with the dual porosity model with the accessible porosity averaged from the Cl^- and Br^- experiments, and the geometrical factor optimized. The porosity in the dual porosity model is larger than in the homogeneous model, in compensation of the decreased mass that is stored in the continuous pores which determines the position of the flux front. Also in compensation of the smaller surface area, the geometrical factors in the dual porosity model are decreased to achieve the same flux at steady state.

The flux front for I^- is retarded compared with that of Cl^- and Br^-. Consequently, the modeled accessible porosity as well as the geometrical factor are higher. A likely explanation for the delayed arrival of I^- relative to the other anions is sorption and a model was constructed with linear sorption of I^-. The model was run with the geomet-

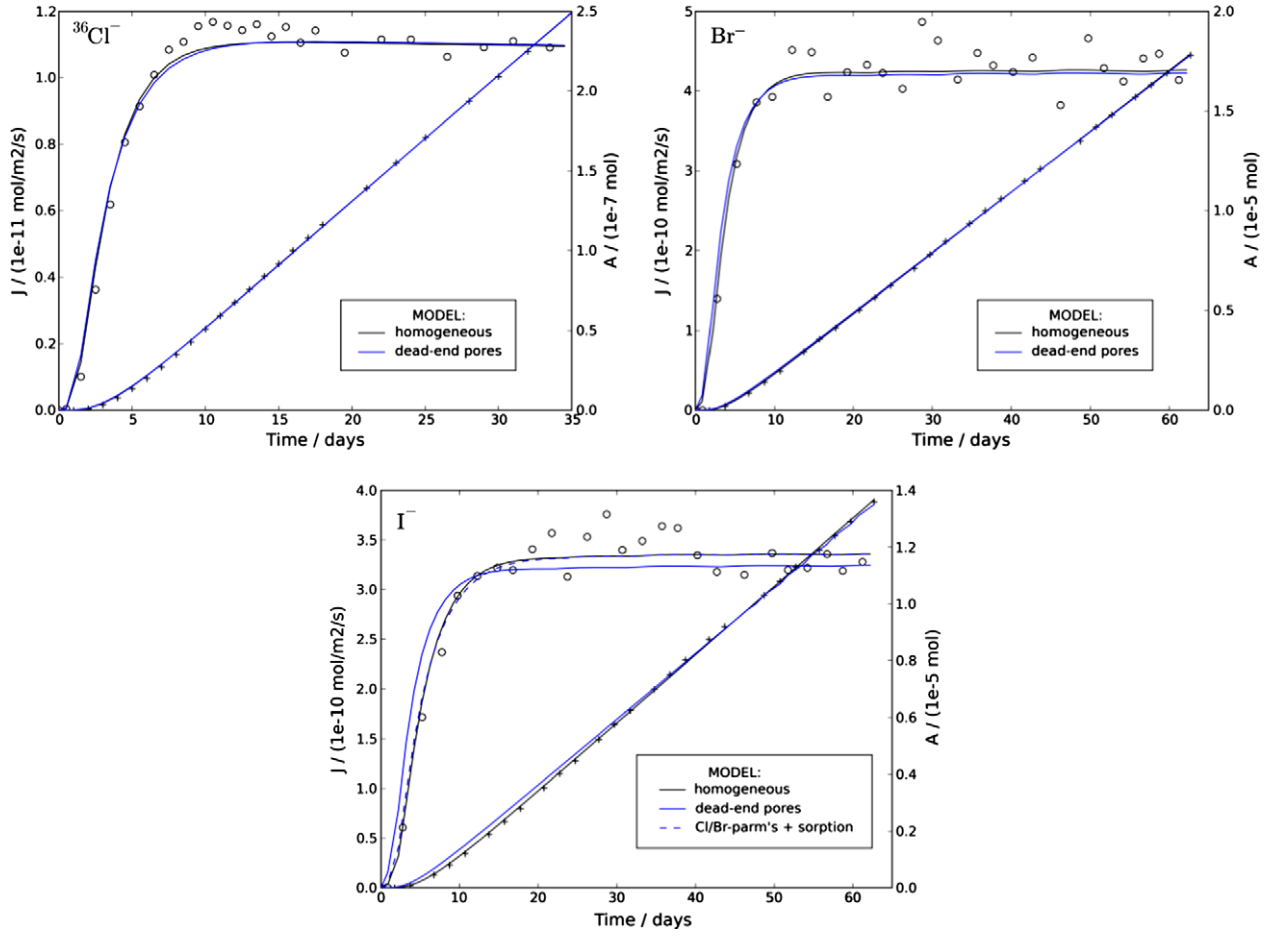

Fig. 5. Cumulative mass outflow (A, + symbols) and corresponding flux (J, o symbols) of anions with model lines for a homogeneous medium (black lines) and for a dual porosity medium with 10% dead-end pores, a porosity of 0.161 and optimized geometrical factor (blue lines). The dashed blue line for I^- results when the dual porosity model, with the averaged accessible porosity from Cl^- and Br^-, is combined with sorption of I^-. (For interpretation of the references to color in this figure legend, the reader is referred to the web version of this article.)

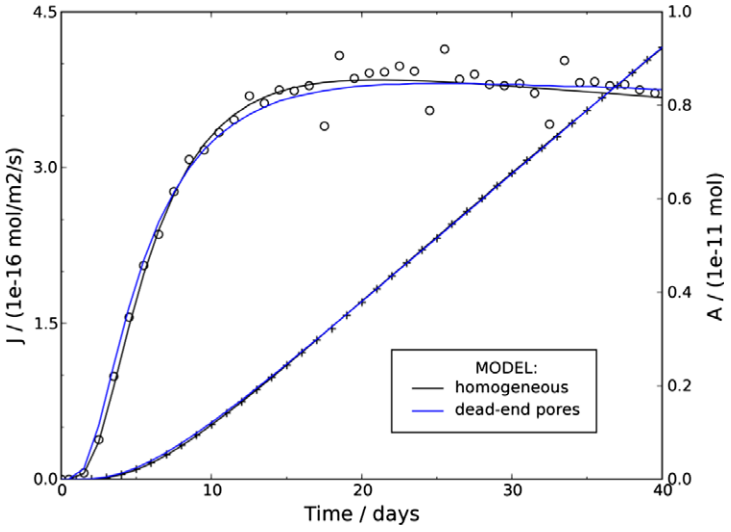

Fig. 6. Cumulative mass outflow (A, + symbols) and corresponding flux (J, o symbols) of $^{22}Na^+$ in the diffusion experiment and model lines for a homogeneous medium and a dual porosity medium.

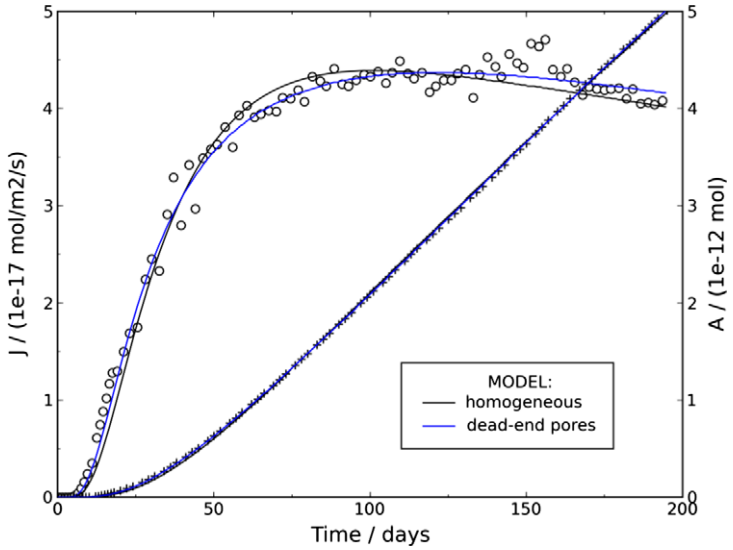

Fig. 7. Cumulative mass outflow (A, + symbols) and corresponding flux (J, o symbols) of $^{85}Sr^{2+}$ in the diffusion experiment and model lines for a homogeneous medium and a dual porosity medium.

rical factor of I^- fixed to the average of Cl^- and Br^- while optimizing the constant for the reaction:

$$I^- + Na^+ + Sor \leftrightarrow SorNaI \quad (13)$$

The results of this model are listed in Table 3, and graphed for the dual porosity model by the dashed blue line in Fig. 5 (overlaps with results from the homogeneous model). In the dead-end pore models, the geometrical factor for I^- is 1.1 times larger than for Cl^- and Br^-, and the reaction constant translates to a distribution coefficient $K_d = 0.02$ (mol/L porewater / mol/L porewater).

3.2. Modeling $^{22}Na^+$ and $^{85}Sr^{2+}$

Data and model lines for $^{22}Na^+$ are shown in Fig. 6. The two models give rather similar fits with the measured data, but small differences in the flux model lines are illustrative for the pitfalls of optimizing highly correlated variables in a natural rock sample. Similar as for anions, a model with dead-end pores results in an earlier front arrival than for the homogeneous case. For anions, this was compensated by increasing the accessible porosity and decreasing geometrical factors. However, for cations the early front arrival can also be compensated by increasing the *CEC*, and data fitting with both *CEC* and geometrical factors as variables results in a reduced geometrical factor for Na^+, similar as for the anions.

The optimized overall *CEC*'s are in the range that has been analyzed in various samples of Opalinus Clay (0.084–0.175 eq/kg, Pearson et al., 2003; 0.10 eq/kg, Lauber et al., 2000). The *CEC*'s of 0.117 eq/kg and 0.124 eq/kg for the homogeneous and dead-end pore models, respectively, agree with measurements close to the sampling site DI-A (cf. Pearson et al., 2003).

The $^{85}Sr^{2+}$ data were fitted using the *CEC*'s found for $^{22}Na^+$, optimizing the geometrical factor and log *K* for the surface complexation reaction. The aqueous complex of $^{85}SrSO_4$ forms about 10% of the tracer concentration and was included with $D_w = 0.4 \times 10^{-9}$ m^2/s and, being a neutral species, with the geometrical factor of HTO. Results of the homogeneous model in Fig. 7 are not entirely satisfactory. The experimental data show a slightly earlier and less steep front arrival, which is typical for dual porosity or kinetic sorption. Kinetic sorption can improve the fit, mainly in the front (model results not shown). However, cation exchange is a very fast reaction, and using kinetics for Sr^{2+} exchange, but not for Na^+, renders this model option unlikely and therefore it is disfavored.

Based on runs with Cs^+ shown next, a dead-end pore structure was defined to occupy 10% of the total porosity (cf. Fig. 1). The exchange among the continuous and dead-end pores was defined by mass-transfer (cf. Parkhurst and Appelo, 1999):

$$mixf_{dead} = \frac{D_p \Delta t A_{dead}}{h V_{dead}} \quad (14)$$

where $mixf_{dead}$ is the mixing factor of continuous and dead-end porewater, Δt is the model time step (s), A_{dead} is the interface of the continuous and the dead-end pores (m^2), assumed equal to the fraction of the radial porous surface of the cell that is occupied by the dead-end pores ($0.1\ \varepsilon\ \pi\ ((r + \Delta r)^2 - r^2)$, with r the radial distance and Δr the cell-size in the model), V_{dead} is the volume of water in the dead-end pores (m^3), and h is the distance between the two regions (m), a factor that was optimized to be $h = 73$ mm. The value of h is larger than the sample height (=52 mm), which indicates that the interfacial area is smaller, or that the porewater diffusion coefficient is smaller than in the continuous pores. However, if also the *CEC* is varied in the two regions as suggested by modeling of the Cs^+ data and the *CEC* is increased in the dead-end pores, the data fitting gives a smaller distance. Also, if the

Table 4
Surface site concentrations and complexation constants for Cs^+ and other alkalis on Opalinus Clay. Su_fes and Su_ii are sites on illite; Su_ (planar) on illite/smectite.

Site type	eq/kg OPA	log $K_{CsSu\_}$	log $K_{NaSu\_}$	log K_{KSu}
Su_fes (frayed edges)	7.40×10^{-5}	17.14	10.0	12.4
Su_ii (intermediate)	7.88×10^{-4}	14.60	10.0	12.1
Su_ (planar)	0.117[a]/0.124[b]	1.34[a]/1.30[b]	−0.7	0.15

[a] Homogeneous.
[b] Dead-end pores models.

exchange rate among the continuous and dead-end pores is small, the model deteriorates markedly for $^{22}Na^+$. After exhaustive trial runs with all the tracers, a value of $h = 52$ mm (the physical maximum) was adopted as a compromise. Further decrease has barely discernible influence on HTO and the anions, and slight effect only on $^{22}Na^+$. For $^{85}Sr^{2+}$, the overall fit improves as illustrated in Fig. 7, and indicated by a 10-fold decrease of the sum of squared errors among the model- and the data points.

3.3. Modeling $^{134}Cs^+$

3.3.1. Sorption isotherm from batch experiments

Sorption of Cs^+ was described by an ion-exchange model (Brouwer et al., 1983; Bradbury and Baeyens, 2000; Zachara et al., 2002; Steefel et al., 2003; Liu et al., 2004). The model discerns three types of sites with different sorption strengths. Strong sites are attributed to the frayed edges of illite, weak sites to the planar (001) faces of illite and montmorillonite, and sites of intermediate strength have an uncertain location. The strong and intermediate sites are occupied by alkali-ions only, while the planar sites sorb all the ions according to the usual ion exchange reactions. The total exchange capacities of the clay of 0.117 or 0.124 eq/kg, obtained from the diffusion experiment with $^{22}Na^+$ for the homogeneous and dead-end pores models, respectively, were attributed to the planar sites. Table 4 presents the numbers optimized on the measured data and Fig. 8 shows the fit. The frayed edge sites become the dominant sorbents when the Cs^+ concentrations are <1 μM, and the planar sites prevail with Cs^+ concentrations >45 μM. For the same experiment, Van Loon et al. (2009) estimated somewhat different numbers, not optimizing for the actually measured data, but using the constants of Bradbury and Baeyens (2000) and the illite content of OPA.

The measurements of the sorption isotherm indicate that the uptake of Cs^+ by the OPA sample is a kinetic process (Van Loon et al., 2009). About 95% of the total sorption took place in the first 30 days. About 99% was sorbed after 260 days and the uptake over that period was used for constructing the isotherm. It is likely that the uptake is a combination of sorption on various surface sites of minerals and slow transformation of K-illite into Cs-illite (Comans et al., 1991; Liu et al., 2003).

3.3.2. Model for $^{134}Cs^+$ diffusion

The measured mass outflow and the calculated flux of Cs^+ are plotted together with model lines in Fig. 9. Comparing the model and flux-data, the model with a homogeneously distributed *CEC* and an adapted geometrical factor shows a delayed front arrival, a relatively high peak and a continuing relatively high flux after the peak (black line). The front can be forced to arrive earlier by decreasing the geometrical factor (dashed black line, 15% smaller geometrical factor). However, with the resulting higher porewater diffusion coefficient of Cs^+, the modeled flux-peak increases even more and the flux after the peak remains too high. The deviations suggest, as for Sr^{2+}, a dual porosity medium in which the continuous pores guide Cs^+ relatively quickly towards the zero-concentration boundary, while part of the mass is taken up by the dead-end pores. A model with 10% dead-end pores has the correct front position and

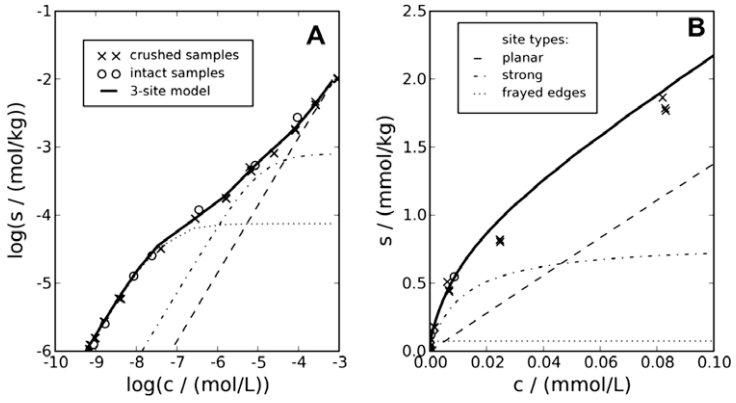

Fig. 8. Sorption isotherm for Cs^+ on Opalinus Clay measured after 260 days and model lines with 3 types of sites. (A) Logarithmic axes, (B) linear axes.

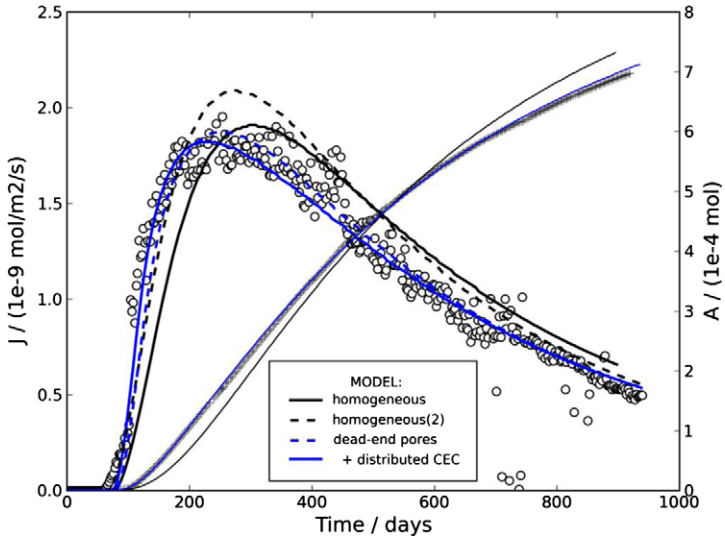

Fig. 9. Cumulative mass outflow (A, + symbols) and corresponding flux (J, o symbols) of Cs^+ in the diffusion experiment and model lines for a homogeneous medium, a dual porosity medium, and a dual porosity medium with kinetics. The dashed black line is for a homogeneous medium with 15% smaller tortuosity than the one displayed by the full black line. The dashed and full blue lines stem from models with 10% dead-end pores and homogeneous or distributed *CEC*, respectively.

shows a reduced peak (dashed blue line). The peak and front position can be improved further by distributing the exchange sites over the domains. The full blue lines show the result when 90% of the average *CEC* is assigned to the continuous pores and the rest to the dead-end pores. Due to rather lengthy computing times, the parameters were obtained by visual fitting only.

4. INTERPRETING THE GEOMETRICAL FACTORS

The model results presented in Table 3 show that the geometrical factors decrease more than 5-fold in the order $I^- > Br^- > {}^{36}Cl^- > HTO > {}^{22}Na^+ > {}^{85}Sr^{2+} > {}^{134}Cs^+$. The geometrical factors for the anions are 1.5 times higher, and for cations 2–4 times smaller than for HTO, which is far more than the experimental uncertainty (cf. Table 3). The decreasing geometrical factors for ${}^{22}Na^+ > {}^{85}Sr^{2+} \geqslant {}^{134}Cs^+$ have no relation with the tracer diffusion coefficients in water (Table 2). However, the decrease follows the order of increasing sorption of the cation, which suggests that diffusion in the diffuse double layer and in the interlayer space plays a role. Accordingly, the variations in the geometrical factors may be explained by considering the diffusional fluxes in these sub domains (Appelo and Wersin, 2007; Leroy et al., 2007; Jougnot et al., 2009).

4.1. Diffusion equations for three porewater fractions

In our interpretation, porewater is subdivided in three fractions, f_{free}, f_{DDL}, and f_{IL} of the total porosity ε_{tot}, representing free porewater, DDL water and interlayer water, respectively (cf. Fig. 1). The flux in free porewater is, according to Eq. (6):

$$J_{free,i} = -f_{free}\varepsilon_{tot}\frac{D_{w,i}}{G_i}\frac{\mathrm{d}c_i}{\mathrm{d}x} \tag{15}$$

Appelo and Wersin (2007) and Jougnot et al. (2009) have shown that the potential gradient in free porewater also applies to diffusion in DDL water, only the concentration being different. Thus, the flux through DDL water follows from Eqs. (1), (2), and (11):

$$J_{DDL,i} = -f_{DDL}\varepsilon_{tot}\frac{D_{w,i}}{G_i}\frac{c_{DDL,i}}{c_i}\frac{\mathrm{d}c_i}{\mathrm{d}x} \tag{16}$$

Since DDL water and free water occupy the same pores, the tortuosity is the same for both fractions. However, in pore constrictions or with a local increase of the surface charge, the constrictivity decreases for anions. Thus, the geometrical factor will appear to increase for anions.

For surface complexed and exchangeable cations, the activity in Eq. (2) is given by the molar or equivalent fraction β_i, which results in:

$$J_{IL,i} = -f_{IL}\varepsilon_{tot}\frac{D_{w,i}}{G_{IL,i}}\frac{c_{IL,i}}{\beta_i}\frac{\mathrm{d}\beta_i}{\mathrm{d}x} \tag{17}$$

where $c_{IL,i}$ is the concentration in interlayer water (mol/L) and G_{IL} is the geometrical factor for interlayer diffusion. In general, for equivalent fractions of exchangeable cations,

$$c_{IL,i} = \frac{\beta_i c_{IL,CEC}}{|z_i|} \tag{18}$$

where $c_{IL,CEC}$ is the *CEC* expressed as concentration in interlayer water (mol/L).

The flux of exchangeable cations then is:

$$J_{IL,i} = -f_{IL}\varepsilon_{tot}\frac{D_{w,i}}{G_{IL,i}}\left(\frac{c_{IL,CEC}}{|z_i|}\right)\frac{\mathrm{d}\beta_i}{\mathrm{d}x} \tag{19}$$

Altogether, the steady state diffusive flux becomes:

$$J_i = -\left\{\frac{\varepsilon_{tot}}{G_i}\left(f_{free} + f_{DDL}\frac{c_{DDL,i}}{c_i}\frac{\eta_{H_2O}}{\eta_{DDL}}\right) + \frac{f_{IL}\varepsilon_{tot}}{G_{IL,i}}\left(\frac{c_{IL,CEC}}{|z_i|}\right)\frac{\mathrm{d}\beta_i}{\mathrm{d}c_i}\right\} \times D_{w,i}\frac{\mathrm{d}c_i}{\mathrm{d}x} \tag{20}$$

where η_{H2O}/η_{DDL} is the viscosity ratio of free porewater and DDL water. The probably different viscosity of interlayer water is included in the geometrical factor G_{IL}.

4.2. Porosity fractions and Donnan potentials

Opalinus Clay contains about 10% illite-smectite mixed layers, dominated by illite (Pearson et al., 2003). It can be calculated that the volume of smectite interlayer water is 2.8 mL/kg clayrock if the smectite forms 3% of the rock and is present as a 1-layer hydrate (with interlayer spacing of 0.25 nm, water density of 1 kg/L, Pitteloud et al., 2000). However, as shown later, interlayer water is probably not measured in diffusion experiments with HTO; it can be neglected except for diffusion of very strongly sorbing cations.

From the accessible porosities of Cl^- and Br^- in the diffusion experiment (Table 3), the anion concentrations in the Donnan volume (Eq. (11)), and neglecting interlayer water, follows the relation between the fraction of free porewater and the potential in the Donnan volume:

$$\frac{\varepsilon_{a,Cl}}{\varepsilon_{tot}} = 0.5 = f_{free} + \left(1 - f_{free}\right)\exp\left(\frac{F\psi_D}{RT}\right) \qquad (21)$$

The relation is shown in Fig. 10A (the python file for calculating Fig. 10 is given in EA-1). The maximal potential is −17 mV for $f_{free} = 0$; it drops rapidly for f_{free} larger than 0.4 and becomes $-\infty$ for $f_{free} = 0.5$. From ψ_D and the concentrations of equally charged ions in free porewater, the free charge of the surface, eq_{Su}, is obtained with Eqs. (11) and (12) which define the Donnan volume. The free surface charge is drawn in Fig. 10B as a function of f_{free}. The *CEC* of OPA (1.7 eq/L porewater) limits f_{free} to be smaller than 0.36.

4.3. Porosity fractions, surface area and -charge, and the association constant K_{NaSu}

It was noted (Section 2.6) that the surface area affects the contribution of the electrostatic term in the surface complexation reaction, and hence, determines the site occupancy and the part of the surface charge that is balanced in the DDL. If both the specific surface area and the complexation constants are known, the site occupancy can be calculated. The remaining surface charge then determines ψ_D, which, in turn, fixes the proportion of free porewater by the measured anion exclusion (Eq. (21)). For a surface area of 37 m^2/g (Section 2.6), the effect of varying log K_{NaSu} is shown in Fig. 10C. With the value for log K_{NaSu} of −0.7 (Section 2.5), f_{free} is 0.117. The corresponding DDL-charge is 45% of the cation exchange capacity (Fig. 10C).

4.4. Comparing estimated and experimental geometrical factors

Neglecting the contribution of interlayer diffusion in Eq. (20), and assuming the same model geometrical factor (G_i) for free and DDL water for all solutes, allows to estimate the overall geometrical factor. The model geometrical factor is estimated with Archie's law, $G_{HTO} = 0.16^{-1} = 6.25$. The resulting overall factors are drawn in Fig. 11 (full lines)

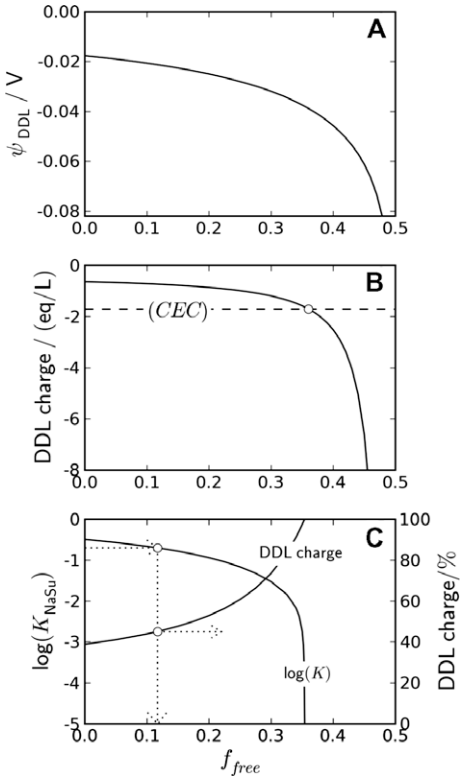

Fig. 10. Relations among f_{free}, the fraction of charge-free porewater and (A) the potential in the DDL; (B) the DDL-charge, also showing the limit of $f_{free} = 0.36$ imposed by the cation exchange capacity; C) log K_{NaSu} and DDL-charge as percentage of *CEC*. Log $K_{NaSu} = -0.7$ fixes f_{free} to 0.117, and the DDL-charge to 45% of the *CEC*.

as a function of f_{free} and the charge number of the solute, with $\eta_{DDL} = \eta_{H2O}$ (Lyklema et al., 1998). For $0 < f_{free} < 0.36$, the geometrical factors vary from 3.1 to 1.6 and from 1.6 to 0.5 for mono- and divalent cations, respectively. The factors for cations decrease with f_{free} since the potential in the Donnan volume lowers to reduce the amounts of anions in the DDL, needed to keep $\varepsilon_{a,Cl} = 0.5\varepsilon_{tot}$ according to Eq. (21). For the anions, the model geometrical factor is equal to the one for HTO, independent of f_{free}, according to Eqs. (20) and (21).

Experimental geometrical factors are plotted in Fig. 11 from the homogeneous model (except for Cs^+ for which only the stagnant model provided a good description of the laboratory experiment; the value from the stagnant model was increased by 10% in compensation of the 10% greater continuous porosity in the homogeneous model). The numbers are also given in Table 5. The value $G_{obs,HTO} = 6.14$, obtained from the diffusion experiments, agrees well with the model value of 6.25 (which is independent of f_{free}). For Na^+, the estimated factor is too high by 1.25; for Sr^{2+} it is too small by 1.25. For Cs^+, the experimental value is much smaller, and for the anions, the experimental values are larger and also different for equally charged anions.

The difference for Na^+ and Sr^{2+} is small but significant relative to the experimental errors, and may be related to porespace configuration. The model geometrical factors

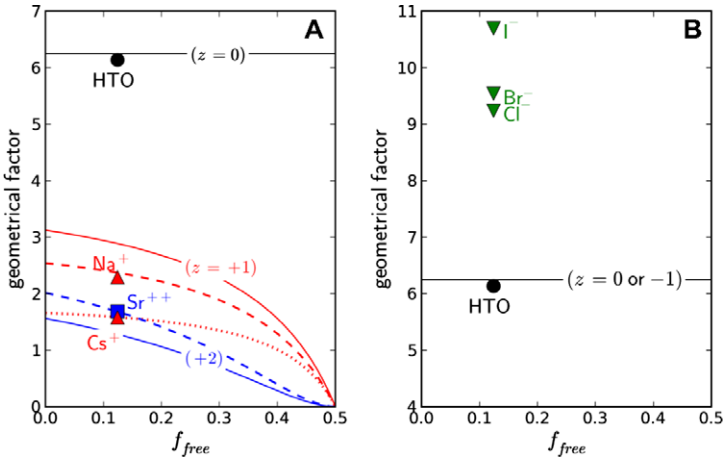

Fig. 11. Estimated and observed geometrical factors for differently charged solutes in Opalinus Clay as a function of f_{free}, the fraction of charge-free porewater of the total porosity. Based on surface area and surface site occupancy, $f_{free} = 0.117$. (A) Full lines give estimated geometrical factors for a pore with free and DDL water; dashed lines include the effect of different ion-pairing of divalent cations and match the observed factors for Na^+ and Sr^{2+}; dotted line includes interlayer diffusion for Cs^+. (B) The estimated geometrical factor is the same for HTO and anions; the observed geometrical factor for anions is 1.5 times higher.

Table 5
Observed and model geometrical factors for differently charged tracers in Opalinus Clay. The observed factor for Cs^+ stems from fitting the data with dead-end pores, multiplied with 1.1 to correct for the larger continuous porosity. The geometrical factor for anions is for an accessible porosity of 0.08. Model numbers for the cations are obtained by stepwise adding diffusion in the DDL, ion-pairing in the DDL, and interlayer diffusion, with the key numbers printed in bold.

	HTO	Na^+	Cs^+	Sr^{++}	Cl^-	Br^-	I^-
G_{obs}	6.14	2.21	1.58[a]	1.68	9.24	9.54	10.7
$G_{\text{model}} = \varepsilon_{\text{tot}}{}^{-1}$	**6.25**						
+ DDL		**2.89**	**2.89**	**1.28**			
+ ion-pairing		2.36	2.36	**1.68**			
+ interlayer diffusion		2.35	**1.58**	1.64			
$G_{\text{overall model}}$	6.25	2.35	1.58	1.64	6.25	6.25	6.25

[a] 1.44×1.1.

are for a uniform pore, with the properties of DDL water defined by the observed anion exclusion. In this pore, a larger fraction of DDL water results in a higher Donnan potential, and thus, in smaller concentration increase of cations in DDL water. In the real medium, the fraction of DDL water may increase in pore constrictions, and keep the same potential if the mineral properties are the same. The concomitant concentration increase of the cations results in smaller apparent geometrical factors. Furthermore, the composition of the DDL is calculated assuming that the dielectric permittivity is the one of bulk water, while it probably decreases (Bockris and Reddy, 1998). A decreasing dielectric permittivity will increase ion-pairing according to Bjerrum theory and reduce the contribution of the divalent cations in DDL water, but increase the role of the less-complexed, monovalent cations.

Following the ion-pairing explanation, the observed geometrical factor for Sr^{2+} is obtained if ion-pairing for Sr^{2+} in DDL water is increased to 32% (whereas it is 10% in free porewater). It requires that the association constant for the $SrSO_4$ ion-pair increases from $10^{2.29}$ to 10^3 in the Donnan volume, or, according to Bjerrum's ion-pairing theory which relates the change to the cube of the dielectric permittivity, that the relative dielectric permittivity of DDL water decreases from 80 to 47. Since the divalent cations show similar ion-pairing in the free solution, mainly with $SO_4{}^{2-}$, the increase will be similar as well. In compensation of the lower contribution of the divalent cations in the DDL, and with the specific composition of free porewater given in Table 2, the concentration of monovalent cations in the DDL increases by 1.23. This concentration increase gives a geometrical factor that is in good agreement with the observed value for Na^+ (dashed line in Fig. 11A; Table 5).

For a very strongly sorbing cation such as Cs^+, the contribution of interlayer or surface diffusion in Eq. (20) is:

$$\frac{f_{\text{IL}}\varepsilon_{tot}}{G_{\text{IL,Cs}}}\left(\frac{c_{\text{IL},CEC}}{1}\right)\frac{\mathrm{d}\beta_{\text{Cs}}}{\mathrm{d}c_{\text{Cs}}} = \frac{0.04\varepsilon_{tot}}{G_{\text{IL,Cs}}}\left(\frac{0.12 \times 0.55}{2.8 \times 10^{-3}}\right) \times 168 = \frac{158\varepsilon_{tot}}{G_{\text{IL,Cs}}} \tag{22}$$

where the term in brackets stands for the *CEC* (=0.12 eq/kg solid), the fraction of the *CEC* occupied by the surface complexes (=0.55) and the volume of interlayer water (=2.8 mL/kg) as given before.

The multiplier for interlayer diffusion of Cs^+ is 158 (Eq. (22)) and much higher than for diffusion through free and DDL water, which varies from 1.9 to 2.1, for $f_{free} = 0$ to 0.13. Since a model that neglects interlayer diffusion approximates the observed overall geometrical factor already, the geometrical factor for interlayer diffusion must be quite high as well, $G_{IL} = 750$ (dotted line in Fig. 11A). For Na^+ and Sr^{2+}, ($d\beta/dc$) is 2 and 9, respectively, or 80–19 times smaller than for Cs^+. Therefore, the contribution of interlayer diffusion is negligible for these cations and for HTO, although it is possible that the mobility of the cations is differently affected by the environment in the interlayer space (Marry et al., 2002; Rotenberg et al., 2007). The stepwise construction of the geometrical factor for the cations with the effects of, first a simple DDL, then different ion-pairing, and finally interlayer diffusion is indicated in Table 5 with numbers in bold for the ion used for calculating the step.

For the anions, the model flux follows from filling the ratio of anion-accessible and total porosity of 0.5 (Eq. (21)) in (20). Accordingly, the flux of the anions is halved relative to the flux of HTO. The observed geometrical factors are at least 50% higher, and increase in the order $Cl^- < Br^- < I^-$. The much higher geometrical factor is readily explained by pore constrictions in which overlapping double layers block transport of anions, while neutral species and cations can pass unhindered or at increased concentrations. The anions must circumnavigate the obstacle, resulting in longer path lengths.

The differences *among* the anions are more difficult to understand. The largest difference, among Cl^- and I^-, is only 15%, but it is significant and has been observed in other experiments as well (Van Loon et al., 2003a,b; Descostes et al., 2008). The difference can be related to ion-pairing with Na^+ which, from electric conductance measurements, is higher for $Cl^- > Br^- > I^-$ (Fuoss, 1980). However, the resulting association constants are rather high. For example, for $NaCl^0$, Fuoss found $K_{NaCl} = 0.82$, which binds 10% of Cl^- in Opalinus Clay porewater in the NaCl complex. Such high ion-pairing could not have gone unnoticed in activity measurements of Na^+ and Cl^- in aqueous systems, but is absent in the databases distributed with PHREEQC (Parkhurst and Appelo, 1999). On the other hand, the relative decrease of the association constants for $NaCl^0$ and NaI^0 of about 20% fits well with the observed decrease of the effective diffusion coefficient of Cl^- and I^-. The different behavior of the anions may also be due to variation of the number and the orientation of the water molecules in the first hydration shell (Wolynes, 1980; Koneshan et al., 1998; Bockris and Reddy, 1998), but this is much more complicated to evaluate and does not offer the simple and straightforward explanation which ion-pairing gives.

5. DISCUSSION

The results show that diffusion of HTO, $^{36}Cl^-$, Br^-, I^-, $^{22}Na^+$, $^{85}Sr^{2+}$ and $^{134}Cs^+$ in a single sample of Opalinus Clay is a function of the accessible porosity, the porewater diffusion coefficient, the cation exchange capacity of the clay, and the exchange constant of the cation. In the literature describing these experiments, the physical and chemical parameters were fitted individually for each tracer. However, in the real situation in the field, interactions among the solutes affect transport and chemical behavior in exchange and mineral reactions. The challenge is thus, to build a model structure that can fit the diffusive transport of the solutes together. The PHREEQC geochemical model offers a framework for that. A structure was devised for Opalinus Clay in which the accessible porosity can be different for anions and for cations and neutral species, in which the solute species can be given different geometrical factors, in which the exchange capacity can be distributed and exchange constants adapted for each cation, in which a dual porosity structure can be introduced, and in which kinetic reactions can be defined. Microscopic observations and analyses indicate that these properties do vary in Opalinus Clay. The question is, of course, how good is the model, and where does it need improvement. But first, the data quality and fitting needs evaluation.

The cumulative out-flowing mass, measured with time in the diffusion experiments, was fitted by model calculations. However, deviations are more evident when the derivative (the flux) is compared with model results. Two duplicate experiments with HTO diverge in the steady state flux. In the 2nd experiment the fitted porosity was 4% smaller than in the first, but since the geometrical factor decreased 7%, the steady state flux was 3% larger. The variation is within the accuracy of the data (1% for HTO(1), 4% for HTO(2)). On the other hand, the properties of the Opalinus Clay sample may have changed during the experiments by oxidation of pyrite with dissolved oxygen in the solutions. Oxidation of pyrite will produce sulfuric acid and possibly iron-oxyhydroxide. The resulting acidification of porewater will dissolve calcite, which may have changed the porosity structure. Also, sorption of iodide may occur on iron-oxyhydroxide which is positively charged at the pH of the solutions. The uncertainty of sample properties and changes therein in the course of the years that the experiments have lasted resides in the model results as well.

A homogeneous model can fit the measured data well by fine-tuning accessible porosities and geometrical factors for HTO and anions, and the exchange capacity for Na^+. The homogeneous models deviate more when the retardation of the cation ($^{85}Sr^{2+}$ and Cs^+) increases. The retardation depends directly on the binding strength of the cation with the clay. Thus, the flux front of $^{85}Sr^{2+}$ arrives in the experiment a few days earlier than the homogeneous model calculates. The front of Cs^+ arrives tens of days sooner in the experiment. Even for $^{22}Na^+$ a small difference may be present. The difference is probably caused by a dual porosity structure of the clay, with continuous and dead-end pores that transmit the tracers differently. Such a dual porosity structure was already described for the diffusion of HTO by Van Loon and Jakob (2005). Also, porosity-heterogeneity is suggested by the irregular distribution of the minerals, which is visible in micro-XRF analyses of Opalinus Clay (Grolimund et al., 2005).

A dual porosity model improves the data fit for $^{85}Sr^{2+}$ and $^{134}Cs^+$. If it is assumed that the physical properties of

the sample have remained the same over time, the proportion of dead-end pores is limited by the fit that can be achieved for HTO, anions and $^{22}Na^{+}$, and then it cannot be more than 10%. However, the oxidation of pyrite and concomitant precipitation of iron-oxyhydroxides may have increased the proportion of dead-end pores in the course of the experiments in which $^{85}Sr^{2+}$ and $^{134}Cs^{+}$ were the last that were done. On the other hand, the dissolution of calcite will increase the connectivity of the pores in the calcite-dominated regions. Thus, the geometrical factor decreases and the effective diffusion coefficient would increase with time. For Cs^{+}, the model may be improved further if the *CEC* in the dead-end pores is larger than in the continuous pores. Since specific sorption of Cs^{+} is linked with illite/montmorillonite, it suggests that the porosity structure of the clay is related to mineralogy, with the calcite-filled areas having a more continuous porosity than the regions where illite dominates.

Diffusion of Cs^{+} has been calculated here with an exchange model based on batch experiments. The exchange constants for Cs^{+} on three site types of different strength are similar to an earlier model for Lauber et al.'s 2000 measurements, and very much the same as the constants found by Steefel et al. (2003). Thus, the different sorption capacities for Cs^{+} in batch- and diffusion experiments that have been invoked before (Van Loon et al., 2004b; Wersin et al., 2007; Maes et al., 2008; Jakob et al., 2009) are unnecessary and in fact, incorrect. The reason for the reported discrepancies lies in the neglect of dead-end pores, but also in the approximate isotherm used in the diffusion model. The plot of the sorption isotherm with linear axes in Fig. 8B illustrates clearly that sorption of Cs^{+} is non-linear. If this non-linear behavior is not correctly incorporated in the diffusion model (for example because model-limitations force to use a simplifying Freundlich isotherm), the sorption capacity may well turn out to become different from the one found in batch experiments since the slope of the isotherm is the important term in the diffusion model, not the integrated mass. Or, with:

$$\frac{\rho_b}{\varepsilon_{a,i}}\frac{\partial s_i}{\partial t} = \frac{\mathrm{d}q_i}{\mathrm{d}c_i}\frac{\partial c_i}{\partial t} \tag{23}$$

in Eq. (7):

$$\frac{\partial c_i}{\partial t} = \frac{D_{p,i}}{(1+\mathrm{d}q_i/\mathrm{d}c_i)}\left(\frac{\partial^2 c_i}{\partial r^2}+\frac{1}{r}\frac{\partial c}{\partial r}\right) \tag{24}$$

where q_i is sorbed concentration per liter porewater. For a very strongly sorbing constituent such as Cs^{+}, an incorrect slope also results in incorrect fitting of the diffusion coefficient.

In the model results, the geometrical factors decrease in the order $I^{-} > Br^{-} > {}^{36}Cl^{-} > HTO > {}^{22}Na^{+} > {}^{85}Sr^{2+} > {}^{134}Cs^{+}$. The decrease is very probably related to the electrochemical properties of a pore, in which part of the porespace is occupied by a double layer. The two-part subdivision of the pore in a fraction of uncharged (f_{free}) and charged water ($f_{DDL} = 1 - f_{free}$) allows to quantify the relations. The quantification requires the measured accessible porosity for anions, the external surface area from BET measurements, the *CEC*, and the association constant of Na^{+} for the surface sites. Of these, the accessible porosity for the halides is the most firmly established by repeated measurements in the laboratory (Van Loon et al., 2003a,b; 2004a) and *in-situ* (Van Loon et al., 2004b; Appelo and Wersin, 2007; Wersin et al., 2007), and it results in at least 45% of the total exchange capacity of Opalinus Clay being located in the DDL. In a similar model for Callovo-Oxfordian clayrock (COX), Leroy et al. (2007), Appelo et al. (2008) and Jougnot et al. (2009) obtained much smaller values of 4–10% for the DDL-charge. However, the water composition in COX (Vinsot et al., 2008) differs from the one in Opalinus Clay. Using Eqs. (11) and (12) that define the DDL water, and a similar anion-accessible porosity of 50% (Gaucher et al., 2006; Descostes et al., 2008), results in 6–11% of the *CEC* being located in the DDL for $0 < f_{free} < 0.3$, in excellent agreement with the earlier findings.

Leroy and Revil (2004) and Leroy et al. (2007) used electrophoretic measurements to estimate the potential of the DDL, and, assuming the fraction of free porewater $f_{free} = 0$, obtained the association constant of Na^{+} for the surface sites that gives the same potential. However, with 0.5 nm Debye length as a measure of the extent of the DDL, and an average pore radius of 4 nm, it is unlikely that the pore is wholly charged. Therefore, we defined the potential of the charged part as a function of f_{free} from the anion-accessible porosity, and used f_{free} as master variable to show the dependency of the various parameters, including the geometrical factor in the diffusion equation. The calculated geometrical factors for Na^{+} and Sr^{2+} can be matched with observed ones, but they do so at a different f_{free}. Apparently, the concentration enhancement of Sr^{2+} in the DDL is less, and of Na^{+} is more. Probably, the difference is related to increased ion-pairing of the divalent cations with SO_4^{2-} in the DDL, due to a smaller dielectric permittivity. The smaller dielectric permittivity of water close to the surfaces of oxides, hydroxides and metals is well established (Bockris et al., 2000; Sverjensky, 2001; Hiemstra and Van Riemsdijk, 2006), and so is the increase of ion-association with decreasing dielectric permittivity of the solution (Fuoss, 1980; Bockris and Reddy, 1998). The effective diffusion coefficient of SO_4^{2-} is equal or half of Cl^{-} in COX (Descostes et al., 2008), while the tracer diffusion coefficient of SO_4^{2-} is half of Cl^{-}. This also suggests that ion-pairing compensates for the increased rejection of the divalent SO_4^{2-} from the DDL (Jougnot et al., 2009).

Ion-pairing in the DDL may also explain the observed, small increase of the geometrical factor for $Cl^{-} < Br^{-} < I^{-}$, which conforms to a small decrease of ion association, in the same order, deduced from electric conductance measurements (Fuoss, 1980). The effect can be included in the equations that relate the electrochemical properties of the pore to f_{free}, which are all based on the observed fraction that the halide anions occupy of the total porespace. It would decrease the calculated DDL potential, and consequently, the maximal f_{free}, that is determined by the *CEC*, decreases. Also the actual f_{free} would decrease that is surmised for Opalinus Clay from pore surface area and the association constants for the surface sites. Consequently (cf. Fig. 11), the difference between the calculated and ob-

served geometrical factor for Sr^{2+} decreases, and less ion-association would be necessary to explain the difference. However, the DDL calculations are done for an average pore, while the increased tortuosity of anions shows that pore constrictions are present that block their transport more than of neutral species and cations. But, it would also mean that transport of higher charged cations is facilitated more than of HTO, and thus, more ion-association is necessary to rationalize the difference with the calculated geometrical factor in which the same tortuosity (path length) is assumed for both HTO and cations.

Still another possibility is that averaging of the DDL properties in a Donnan volume accounts insufficiently for the different enrichment of cations near the surface, and the associated different diffusion along it. For example, the larger hydrated radius of Sr^{2+} and the smaller one of Cs^+, relative to Na^+, will decrease, respectively increase diffusion relative to Na^+, compared with the average that is calculated for a Donnan volume. However, it can be calculated by numerical integration (cf. Appelo and Postma, 2005) that the closer approach to the surface of Cs^+ is not enough for explaining its higher diffusion, and surface or interlayer diffusion is likely for this ion. This process has a rather high geometrical factor of 840, which reduces the effective diffusion coefficient to 2×10^{-12} m^2/s, or 100 times smaller than calculated with molecular dynamics simulations (MD) for the interlayer space of montmorillonite with a single layer of water (Chang et al., 1995; Marry et al., 2002; Rotenberg et al., 2007; Liu et al., 2008). Of course, the MD number is for a small rectangular box, without the irregular stacking and distribution of montmorillonite in mixed layers of illite and montmorillonite in a natural clayrock. From the small diffusion coefficient for Cs^+, we inferred that the contribution of interlayer or surface diffusion would be insignificant for cations with a much smaller distribution coefficient than that of Cs^+. Furthermore, it was assumed that water in the Donnan volume has the viscosity of free porewater, although it may be somewhat higher (Lyklema et al., 1998). With a higher viscosity for DDL water, the diffusion enhancement is less for cations, a higher proportion of the Cs^+ flux is then apportioned to interlayer diffusion, and the geometrical factor for interlayer diffusion would decrease.

6. CONCLUSIONS

A dual porosity model can calculate, concomitantly, diffusion of tritium, anions, and cations in a sample of Opalinus Clay in close agreement with experimental data. The dual porosity structure is needed for $^{85}Sr^{2+}$ and $^{134}Cs^+$, but $^{22}Na^+$, tritium and the anions can be modeled as well or even better with a homogeneous porosity structure. The fraction of dead-end pores is limited to about 10%, but modeling indicates that this fraction contains a relatively greater share of about 19% of the total exchange capacity of the clay sample. It is possible that the porosity structure has been influenced by pyrite oxidation occurring in the course of the experiment. Hence, the access of oxygen should be avoided in future experiments. The model is able to describe the diffusion of Cs^+ using measured sorption data as input for an exchange model with three sites of different strengths. Thus, it is unnecessary to assume a smaller sorption capacity for diffusion than measured in batch experiments and to adapt the geometrical factor of Cs^+ to fit diffusion data, as was suggested by Maes et al. (2008).

The diffusion behavior is summarized in different geometrical factors for differently charged solutes. The differences are related to the electrochemical properties of the pore which can be approximated by a bipartition of porewater in a free, uncharged part, and a DDL averaged in a Donnan volume. The geometrical factor of tritium (HTO) is given by the inverse of the porosity, in fair agreement with Archie's law. Cations and HTO travel along the same paths, and the geometrical factor should be the same. However, diffusion of cations is enhanced by their concentration increase in the Donnan volume. This increase is affected by ion-pairing in the Donnan volume due to the smaller dielectric permittivity in the DDL. More ion-pairing reduces the concentration increase of the divalent cations whereas it increases the concentrations of the monovalent cations, which explains the observed behavior of Na^+ and Sr^{2+}. Interlayer or surface diffusion contributes to diffusion of strongly sorbed cations such as Cs^+.

Anions are partially excluded from the Donnan volume, which results in slower diffusion than of HTO. A simple formula gives the decline as the fraction of the total porosity that is accessible for anions. The actual decrease is higher because pore constrictions with overlapping DDLs force the anions to take longer routes in the clayrock. Small differences among the halide anions are also related to different ion-pairing in the DDL.

The geometrical factors for cations can be quantified as a function of the fraction of free porewater in the porespace and a given anion-accessible porosity. For a particular clayrock, the fraction of free porewater is determined by the porewater composition, the pore diameter, the cation exchange capacity, and the association constants for the surface sites. It allows to estimate porewater diffusion coefficients for cations, to be corrected for ion-pairing using the relative dielectric permittivity of about 50 that was found in this study.

ACKNOWLEDGEMENTS

The authors like to thank Nagra, Andra and the Mont Terri Project for financial support. The technical assistance of Werner Müller during the experiments is greatly appreciated.

APPENDIX A. SUPPLEMENTARY DATA

Supplementary data associated with this article can be found, in the online version, at doi:10.1016/j.gca.2009.11.013.

REFERENCES

Appelo C. A. J. and Postma D. (2005) *Geochemistry, Groundwater and Pollution*, second ed. Balkema, Leiden, 649 p.

Appelo C. A. J. and Wersin P. (2007) Multicomponent diffusion modeling in clay systems with application to the diffusion of

tritium, iodide and sodium in Opalinus Clay. *Environ. Sci. Technol.* **41**, 5002–5007.

Appelo C. A. J., Vinsot A., Mettler S. and Wechner S. (2008) Obtaining the porewater composition of a clay rock by modeling the in- and out-diffusion of anions and cations from an in-situ experiment. *J. Contam. Hydrol.* **101**, 67–76.

Bockris J. O'M. and Reddy A. K. N. (1998) *Modern Electrochemistry: Ionics*, second ed. Plenum Press, New York, 767 p.

Bockris J. O'M., Reddy A. K. N., Gamboa-Aldeco M., Bockris J. O'M., Reddy A. K. N. and Gamboa-Aldeco M. (2000) *Modern electrochemistry: fundamentals of electrodics*. Kluwer/Plenum Publ., New York, p. 771–1534.

Bolt G. H. and De Haan F. A. M. (1982) Anion exclusion in soil. In *Soil Chemistry, B. Physico-Chemical Models* (ed. G. H. Bolt). Elsevier, Amsterdam, pp. 233–257.

Boudreau B. P. (1997) *Diagenetic models and their implementation*. Springer, Berlin, 414 p.

Bourg I. C. (2004) Tracer diffusion of water and inorganic ions in compacted saturated sodium bentonite. Ph.D. Thesis, Univ. Cal., Berkeley, 368 p.

Bourg I. C., Sposito G. and Bourg A. C. M. (2007) Modeling cation diffusion in compacted water-saturated sodium bentonite at low ionic strength. *Environ. Sci. Technol.* **41**, 8118–8122.

Bradbury M. H. and Baeyens B. (2000) A generalised sorption model for the concentration dependent uptake of Cs by argillaceous rocks. *J. Contam. Hydrol.* **42**, 141–163.

Bradbury M. H. and Baeyens B. (2003) Porewater chemistry in compacted re-saturated MX-80 bentonite. *J. Contam. Hydrol.* **61**, 329–338.

Brouwer E., Baeyens B., Maes A. and Cremers A. (1983) Cesium and rubidium ion equilibria in illite clay. *J. Phys. Chem.* **87**, 1213–1219.

Chang F.-R., Skipper N. T. and Sposito G. (1995) Computer simulation of interlayer molecular structure in sodium montmorillonite hydrates. *Langmuir* **11**, 2734–2741.

Comans R. N. J., Haller M. and De Preter P. (1991) Sorption of cesium on illite: non-equilibrium behaviour and reversibility. *Geochim. Cosmochim. Acta* **55**, 433–440.

Croisé J., Schlickenrieder L., Marschall P., Boisson J.-Y., Vogel P. and Yamamoto S. (2004) Hydrogeological investigations in a low permeability claystone formation: the Mont Terri Rock Laboratory. *Phys. Chem. Earth* **29**, 3–15.

Descostes M., Blin V., Bazer-Bachi F., Meier P., Grenut B., Radwan J., Schlegel M. L., Buschaert S., Coelho D. and Tevissen E. (2008) Diffusion of anionic species in Callovo-Oxfordian argillites and Oxfordian limestones (Meuse/Haute–Marne, France). *Appl. Geochem.* **23**, 655–677.

Doherty J. (1994) PEST, Model-independent parameter estimation. Available from: <http://www.sspa.com/pest/download.html>.

Dullien F. A. L. (1992) *Porous Media*, second ed. Academic Press, San Diego, 574 p.

Dzombak D. A. and Morel F. A. A. (1990) *Surface complexation modeling: hydrous ferric oxide*. Wiley and Sons, New York, 393 p.

Dzombak D. A. and Hudson R. J. M. (1995) Ion exchange: the contributions of diffuse layer sorption and surface complexation. *Adv. Chem. Ser.* **244**, 59–94.

Eriksen T. E., Jansson M. and Molera M. (1999) Sorption effects on cation diffusion in compacted bentonite. *Eng. Geol.* **54**, 231–236.

Fuoss R. M. (1980) Conductimetric determination of thermodynamic pairing constants for symmetrical electrolytes. *Proc. Natl. Acad. Sci. USA* **77**, 34–38.

Gaucher E. C., Blanc P., Bardot F., Braibant G., Buschaert S., Crouzet C., Gautier A., Girard J.-P., Jacquot E., Lassin A., Negrel G., Tournassat C., Vinsot A. and Altmann S. (2006) Modelling the porewater chemistry of the Callovo-Oxfordian formation at a regional scale. *C.R. Acad. Geosci.* **338**, 917–930.

Gimmi T. (2003) Porosity, pore structure, and energy state of porewater of Opalinus Clay from Benken. Int. Ber. 03–09, NAGRA, Wettingen, 114 p.

Glaus M. A., Baeyens B., Bradbury M. H., Jakob A., Van Loon L. R. and Yaroshchuk A. (2007) Diffusion of ^{22}Na and ^{85}Sr in montmorillonite: Evidence of interlayer diffusion being the dominant pathway at high compaction. *Eviron. Sci. Technol.* **41**, 478–485.

Glaus M. A., Rossé R., Van Loon L. R. and Yaroshchuk A. (2008) Tracer diffusion in sintered stainless steel filters: measurement of effective diffusion coefficients and implications for diffusion studies in compacted clay minerals. *Clays Clay. Miner.* **56**, 677–685.

Grathwohl P. (1998) *Diffusion in Porous Media*. Springer, Berlin, 207 p.

Grolimund D., Günther D., Scheidegger A. M., Aeschlimann B., Wersin P. and Heald S. M. (2005) Cs migration in complex geological media: new insights through micro-imaging and micro-spectroscopy. In *Clays in Natural & Engineered Barriers for Radioactive Waste Confinement. 2nd International Meeting*, March 14–18, 2005, Tours, France.

Hiemstra T. and Van Riemsdijk W. H. (2006) On the relationship between charge distribution, surface hydration, and the structure of the interface of metal hydroxides. *J. Colloid Interface Sci.* **301**, 1–18.

Jakob A., Pfingsten W. and Van Loon L. (2009) Effects of sorption competition on caesium diffusion through compacted argillaceous rock. *Geochim. Cosmochim. Acta* **73**, 2441–2456.

Jougnot D., Revil A. and Leroy P. (2009) Diffusion of ionic tracers in the Callovo-Oxfordian clay-rock using the Donnan equilibrium model and the formation factor. *Geochim. Cosmochim. Acta* **73**, 2712–2726.

Kemper W. D. and Quirk J. P. (1972) Ion mobilities and electric charge of external clay surfaces inferred from potential differences and osmotic flow. *Soil Sci. Soc. Am. Proc.* **36**, 426–433.

Koneshan S., Rasaiah J. C., Lynden-Bell R. M. and Lee S. H. (1998) Solvent structure, dynamics, and ion mobility in aqueous solutions at 25 °C. *J. Phys. Chem. B* **102**, 4193–4204.

Kozaki T., Saito N., Fujishima A., Sato S. and Ohashi H. (1998) Activation energy for diffusion of chloride ions in compacted sodium montmorillonite. *J. Contam. Hydrol.* **35**, 67–75.

Kozaki T., Fujishima A., Saito N., Sato S. and Ohashi H. (2005) Effects of dry density and exchangeable cations on the diffusion process of sodium ions in compacted montmorillonite. *Eng. Geol.* **81**, 246–254.

Kozaki T., Liu J. and Sato S. (2008) Diffusion mechanism of sodium ions in compacted montmorillonite under different NaCl concentration. *Phys. Chem. Earth* **33**, 957–961.

Lauber M., Baeyens B. and Bradbury M. H. (2000) Physico-chemical characterisation and sorption measurements of Cs, Sr, Ni, Eu, Th, Sn and Se on Opalinus Clay from Mont Terri. PSI Bericht 00-11, Paul Scherrer Institut, Villigen, Swizerland, 78 p.

Lehikoinen J., Muurinen A. and Valkiainen M. (1999) A consistent model for anion exclusion and surface diffusion. *Mat. Res. Soc. Symp.* **556**, 663–670.

Leroy P. and Revil A. (2004) A triple-layer model of the surface electrochemical properties of clay minerals. *J. Colloid Interface Sci.* **270**, 371–380.

Leroy P., Revil A. and Coelho D. (2006) Diffusion of ionic species in bentonite. *J. Colloid Interface Sci.* **296**, 248–255.

Leroy P., Revil A., Altmann S. and Tournassat C. (2007) Modeling the composition of the pore water in a clay–rock geological formation (Callovo-Oxfordian, France). *Geochim. Cosmochim. Acta* **71**, 1087–1097.

Liu C., Zachara J. M., Smith S. C., Mckinley J. P. and Ainsworth C. C. (2003) Desorption kinetics of radiocesium from subsurface sediments at Hanford Site, USA. *Geochim. Cosmochim. Acta* **67**, 2893–2912.

Liu C., Zachara J. M. and Smith S. C. (2004) A cation exchange model to describe Cs^+ sorption at high ionic strength in subsurface sediments at Hanford site, USA. *J. Contam. Hydrol.* **68**, 217–238.

Liu X., Lu X., Wang R. and Zhou H. (2008) Effects of layer-charge distribution on the thermodynamic and microscopic properties of Cs-smectite. *Geochim. Cosmochim. Acta* **72**, 1837–1847.

Lyklema J., Rovillard S. and De Coninck J. (1998) Electrokinetics: the properties of the stagnant layer unraveled. *Langmuir* **14**, 5659–5663.

Maes N., Salah S., Jacques D., Aertsens M., Van Gompel M., De Cannière P. and Velitchkova N. (2008) Retention of Cs in Boom Clay: comparison of data from batch sorption tests and diffusion experiments on intact clay cores. *Phys. Chem. Earth* **33**, S149–S155.

Marry V., Turq P., Cartailler T. and Levesque D. (2002) Microscopic simulation of structure and dynamics of water and counterions in a monohydrated montmorillonite. *J. Chem. Phys.* **117**, 3454–3463.

Melkior T., Yahiaoui S., Thoby D., Motellier S. and Barthès V. (2007) Diffusion coefficients of alkaline cations in Bure mudrock. *Phys. Chem. Earth* **32**, 453–462.

Molera M. and Eriksen T. (2002) Diffusion of $^{22}Na^+$, $^{85}Sr^{2+}$, $^{134}Cs^+$ and $^{57}Co^{2+}$ in bentonite clay compacted to different densities: experiments and modeling. *Radiochim. Acta* **90**, 753–760.

Muurinen A., Karnland O. and Lehikoinen J. (2004) Ion concentration caused by an external solution into the porewater of compacted bentonite. *Phys. Chem. Earth* **29**, 119–127.

Muurinen A., Karnland O. and Lehikoinen J. (2007) Effect of homogenization on the microstructure and exclusion of chloride in compacted bentonite. *Phys. Chem. Earth* **32**, 485–490.

Nagra (2002a) Project Opalinus clay. Safety report: demonstration of disposal feasibility for spent fuel, vitrified high-level waste and long-lived intermediate-level waste (Entsorgungsnachweiss). Nagra Technical Report NTB 02–05, Wettingen, Switzerland.

Nagra (2002b) Projekt Opalinuston: synthese der geowissenschaftlichen Untersuchungsergebnisse. Nagra Technical Report NTB 02–03, Nagra, Wettingen, Switzerland.

Ochs M., Boonekamp M., Wanner H., Sato H. and Yui M. (1998) A quantitative model for ion diffusion in compacted bentonite. *Radiochim. Acta* **82**, 437–443.

Ochs M., Lothenbach B., Wanner H., Sato H. and Yui M. (2001) An integrated sorption–diffusion model for the calculation of consistent distribution and diffusion coefficients in compacted bentonite. *J. Contam. Hydrol.* **47**, 283–296.

Ohlsson Y. and Neretnieks I. (1998) Some evidence for surface ion mobility in rock. *J. Contam. Hydrol.* **35**, 91–100.

Palut J.-M., Montarnal P., Gautschi A., Tevissen E. and Mouche M. (2003) Characterisation of HTO diffusion properties by an in situ tracer experiment in Opalinus Clay at Mont Terri. *J. Contam. Hydrol.* **61**, 203–218.

Parkhurst D. L. and Appelo, C. A. J. (1999) User's guide to PHREEQC (version 2). US Geol. Surv. Water Resour. Inv. Rep. 99-4259.

Pearson F. J. (1998) Opalinus Clay experimental water: A1 Type, Version 980318. Technical Report TM-44-98-07. Paul Scherrer Institute, Villigen Switzerland.

Pearson F. J., Arcos D., Bath A., Boisson J. Y., Fernández A. M., Gäbler H. E., Gaucher E., Gautschi A., Griffault L., Hernán P. and Waber H. N. (2003) Geochemistry of water in the Opalinus Clay formation at the Mont Terri rock laboratory. *Report of the Swiss Federal Office for Water and Geology, Geology Series* 5, 319 p.

Pitteloud C., Powell D. H., Soper A. K. and Benmore C. J. (2000) The structure of interlayer water in Wyoming montmorillonite studied by neutron diffraction with isotopic substitution. *Physica B* **276–278**, 236–237.

Rotenberg B., Marry V., Dufrêche J.-F., Malikova N., Giffaut E. and Turq P. (2007) Modelling water and ion diffusion in clays: a multiscale approach. *CR Chimie* **10**, 1108–1116.

Sato H. (2005) Effects of the orientation of smectite particles and ionic strength on diffusion and activation enthalpies of I^- and Cs^+ ions in compacted smectite. *Appl. Clay Sci.* **29**, 267–281.

Sato H., Ashida T., Kohara Y., Yui M. and Sasaki M. (1992) Effect of dry density on diffusion of some radionuclides in compacted sodium bentonite. *J. Nucl. Sci. Technol.* **29**, 873–882.

Shackelford C. D. and Daniel D. E. (1991) Diffusion in saturated soil. II: results for compacted clay. *J. Geotechn. Eng.* **117**, 485–506.

Steefel C. I., Carroll S. A., Zhao P. and Roberts S. (2003) Cesium migration in Hanford sediment: a multisite cation exchange model based on laboratory transport experiments. *J. Contam. Hydrol.* **67**, 219–246.

Sverjensky D. A. (2001) Interpretation and prediction of triple-layer model capacitances and the structure of the oxide–electrolyte–water interface. *Geochim. Cosmochim. Acta* **65**, 3643–3655.

Thury M. and Bossart P. (1999) The Mont Terri rock laboratory, a new international research project in a Mesozoic shale formation. *Eng. Geol.* **52**, 347–359.

Van Brakel J. and Heertjes P. M. (1974) Analysis of diffusion in macroporous media in terms of a porosity, a tortuosity and a constrictivity factor. *Int. J. Heat Mass Transfer* **17**, 1093–1103.

Van Loon L. R., Soler J. M. and Bradbury M. H. (2003a) Diffusion of HTO, $^{36}Cl^-$ and $^{125}I^-$ in Opalinus Clay samples from Mont Terri: effect of confining pressure. *J. Contam. Hydrol.* **61**, 73–83.

Van Loon L. R., Soler J. M., Jakob A. and Bradbury M. H. (2003b) Effect of confining pressure on the diffusion of HTO, $^{36}Cl^-$ and $^{125}I^-$ in a layered argillaceous rock (Opalinus Clay): diffusion perpendicular to the fabric. *Appl. Geochem.* **18**, 1653–1662.

Van Loon L. R., Soler J. M., Müller W. and Bradbury M. H. (2004a) Anisotropic diffusion in layered argillaceous formations: a case study with Opalinus clay. *Environ. Sci. Technol.* **38**, 5721–5728.

Van Loon L. R., Wersin P., Soler J. M., Eikenberg J., Gimmi Th., Hernán P., Dewonck S. and Savoye S. (2004b) *In-situ* diffusion of HTO, $^{22}Na^+$, Cs^+ and I^- in Opalinus Clay at the Mont Terri underground rock laboratory. *Radiochim. Acta* **92**, 757–763.

Van Loon L. R. and Soler J. M. (2004) Diffusion of HTO, $^{36}Cl^-$ and $^{22}Na^+$ in Opalinus Clay: effect of confining pressure, sample orientation, sample depth and temperature. PSI Bericht 04–03, Paul Scherrer Institut, Villigen, Switzerland. Also published as Nagra NTB 03–07, Nagra, Wettingen, Switzerland.

Van Loon L. R. and Jakob A. (2005) Evidence for a second transport porosity for the diffusion of tritiated water (HTO) in a sedimentary rock (Opalinus Clay – OPA): Application of through- and out-diffusion techniques. TIPM 61, pp.193–214.

Van Loon L. R., Baeyens B. and Bradbury M. H. (2005) Diffusion and retention of sodium and strontium in Opalinus Clay: comparison of sorption data from diffusion and batch sorption measurement, and geochemical calculations. *Appl. Geochem.* **20**, 2351–2363.

Van Loon L. R., Glaus M. A. and Müller W. (2007) Anion exclusion effects in compacted bentonites: towards a better understanding of anion diffusion. *Appl. Geochem.* **22**, 2536–2552.

Van Loon L. R., Baeyens B. and Bradbury M. H. (2009) The sorption behaviour of caesium on Opalinus Clay: a comparison between intact and crushed material. *Appl. Geochem.* **24**, 999–1004.

Van Schaik J. C., Kemper W. D. and Olsen S. R. (1966) Contribution of adsorbed cations to diffusion in clay–water systems. *Soil Sci. Soc. Am. Proc.* **30**, 17–22.

Vinsot A., Mettler S. and Wechner S. (2008) In situ characterization of the Callovo-Oxfordian pore water composition. *Phys. Chem. Earth* **33**, S75–S86.

Wersin P., Van Loon L. R., Soler J. M., Yllera A., Eikenberg J., Gimmi T., Hernán P. and Boisson J.-Y. (2004) Long-term diffusion experiment at Mont Terri: first results from field and laboratory data. *Appl. Clay Sci.* **26**, 123–135.

Wersin P., Soler J. M., Van Loon L., Eikenberg J., Baeyens B., Grolimund D., Gimmi T. and Dewonck S. (2007) Diffusion of HTO, Br^-, I^-, Cs^+, $^{85}Sr^{2+}$ and $^{60}Co^{2+}$ in a clay formation: results and modelling from an in situ experiment in Opalinus Clay. *Appl. Geochem.* **23**, 678–691.

Wolynes P. G. (1980) Dynamics of electrolyte solutions. *Ann. Rev. Phys. Chem.* **31**, 345–376.

Zachara J. M., Smith S. C., Liu C. X., McKinley J. P., Serne R. J. and Gassman P. L. (2002) Sorption of Cs^+ to micaceous subsurface sediments from the Hanford site. *Geochim. Cosmochim. Acta* **66**, 193–211.

Associate editor: Eric H. Oelkers

Supplementary Information to:

C.A.J. Appelo, L.R. Van Loon and P.Wersin: Multicomponent diffusion of a suite of tracers (HTO, Cl, Br, I, Na, Sr, Cs) in a single sample of Opalinus Clay.

This supplementary information contains:
1) A table with the experimental times for the individual tracer tests;
2) A python input file for plotting Figure 10 with matplotlib, illustrating how various parameters in the surface complexation/diffusion model are calculated;
3) A c-program that prints the PHREEQC-2 input file for calculating diffusion of Cs^+ in the radial setup.

1) Experimental times for the individual tracer tests.

Tracer	Through-diffusion			Out-diffusion		
	start	end	Time (days)	start	end	Time (days)
HTO-1	3/12/2001	21/12/2001	18	21/12/2001	2/4/2002	102
HTO-2	3/4/2002	6/5/2002	33	7/5/2002	12/8/2002	98
Cl-36	19/8/2002	23/9/2002	35	23/9/2002	22/1/2003	121
Na-22	23/1/2003	4/3/2003	41	4/3/2003	21/11/2003	262
Sr-85	25/11/2003	7/6/2004	195	7/6/2004	7/3/2005	273
I/Br	8/3/2005	9/5/2005	63	-	-	-
Cs-134	10/5/2005	ongoing				

2) Python input file for plotting Figure 10 with Matplotlib.

```
# Plots Fig. 10 : Psi_DDL, DDL_charge and log(K_NaSu) as a function of
#       f_free, the fraction of free porewater

# total porosity, anion-accesible porosity, interlayer porosity...
eps_tot = 0.16; eps_an = 0.08; f_IL = 0.0
RT_F = 296.0 / 298 * 0.02569;

# fill vectors with f_free, psi_DDL and the Boltzmann factor...
f_free = [];
psi = [];
BM_factor = [];

for i in range(0, 49):
       f_free.append(i / 100.0);

for i in range(0, 49):
       a = log( (eps_an / eps_tot - f_free[i]) / (1 - f_free[i] - f_IL)) * RT_F;
       psi.append( a );
       BM_factor.append( exp(-a / RT_F));

# calculate the DDL_charge...
#        +1     +2      -1      -2   charge groups in OPA water
eq_L = [0.239, 0.078, -0.303, -0.016]
DDL_charge = [];

for i in range(0, 49):
       a1 = -(eq_L[0] * BM_factor[i] + eq_L[1] * BM_factor[i]**2 + eq_L[2] / BM_factor[i] +
eq_L[3] / BM_factor[i]**2) * (1 - f_free[i] - f_IL);
       DDL_charge.append( a1 );

# log(K_NaSu) was optimized with PHREEQC/PEST to get the target psi for a set of f_free
values...
```

```
f_free2  =  [1.000E-04,  5.000E-02,  1.000E-01,  1.173E-01,  1.500E-01,  1.750E-01,  2.000E-01,
2.250E-01,  2.500E-01,  2.750E-01,  3.000E-01,  3.250E-01,  3.400E-01,  3.450E-01,  3.500E-01,
3.520E-01, 3.530E-01, 3.54E-01];
lgKNaSu = [-4.937E-01, -5.688E-01, -6.621E-01, -7.000E-01, -7.814E-01, -8.547E-01, -9.401E-01,
-1.041E+00,  -1.164E+00,  -1.319E+00,  -1.524E+00,  -1.834E+00,  -2.168E+00,  -2.364E+00,  -
2.732E+00, -3.079E+00, -3.507E+00, -5E+00];
DDL_charge2 = [3.894E+01, 4.112E+01, 4.394E+01, 4.511E+01, 4.770E+01, 5.009E+01, 5.295E+01,
5.640E+01,  6.073E+01,  6.628E+01,  7.351E+01,  8.337E+01,  9.117E+01,  9.419E+01,  9.747E+01,
9.886E+01, 9.958E+01, 9.994E+01];

from matplotlib import rcParams
rcParams['legend.fontsize'] = 12
rcParams['figure.figsize'] = 5, 8 # figure in inches
from matplotlib.ticker import MultipleLocator

figure(1); clf()

# psi vs f_free...
ax = axes([0.2, 0.71, 0.6, 0.25]);
plot(f_free, psi, 'k-', lw = 1)
# ticmarks and text...
ax.yaxis.set_major_locator(MultipleLocator(0.02))
say = r'$\sf{\psi_{\ DDL}\ /\ V}$'
ylabel(say, size = 16);
sax = r'$\it{f_{free}}$'
text(0.47, -0.008, 'A', fontsize = 15);
plot([0.477], [-0.005], 'o', mfc='w', ms = 16);
axis([0, 0.5, -0.082, 0])

# DDL charge vs f_free...
ax = axes([0.2, 0.4, 0.6, 0.25]);
plot(f_free, DDL_charge, 'k-', lw = 1);
# ticmarks and text...
ax.yaxis.set_major_locator(MultipleLocator(2))
say = r'$\sf{DDL\ charge\ /\ (eq/L)}$'
ylabel(say, size = 16);
plot([0, 0.5], [-1.7, -1.7], 'k--');
plot([0.36], [-1.7], 'o', mfc='w');
text(0.47, -0.8, 'B', fontsize = 15);
plot([0.477], [-0.5], 'o', mfc='w', ms = 16);
axis([0, 0.5, -8, 0]);
s = r'$(\it{CEC})$';
text(0.1, -2.25, s, fontsize = 15, bbox=dict(edgecolor='w', facecolor = 'w'));

# lgKNaSu vs f_free...
ax = axes([0.2, 0.09, 0.6, 0.25]);
plot(f_free2, lgKNaSu, 'k-', lw = 1);
ax.yaxis.set_major_locator(MultipleLocator(1))
say = r'$\sf{log(\it{K}_{\sf{NaSu}})}$'
ylabel(say, size = 16);
xlabel(sax, size = 16);
plot([0, 0.1173], [-0.7, -0.7], 'k:');
plot([0.10, 0.1173, 0.10], [-0.51, -0.7, -0.89], 'k:');
plot([0.1173, 0.1173], [-0.7, -5], 'k:');
plot([0.101, 0.1173, 0.133], [-4.72, -5, -4.7], 'k:');
plot([0.1173], [-0.7], 'o', mfc='w');
s2 = r'$\sf{log(\it{K})}$'
text(0.32, -4, s2, fontsize = 12, bbox=dict(edgecolor='w', facecolor = 'w'));
axis([0, 0.5, -5, 0]);

# % DDL charge on the 2nd y-axis...
ax2 = twinx()
plot(f_free2, DDL_charge2, 'k-', lw = 1);
plot([0.1173, 0.22], [45, 45], 'k:');
plot([0.204, 0.22, 0.204], [48, 45, 42], 'k:');
plot([0.1173], [45.1], 'o', mfc='w');
say2 = r'$\sf{DDL\ charge / \%}$'
ylabel(say2, size = 16);
s3 = r'$\sf{DDL\ charge}$'
text(0.28, 79, s3, fontsize = 12, bbox=dict(edgecolor='w', facecolor = 'w'));
plot([0.477], [94], 'o', mfc='w', ms = 16);
text(0.47, 90, 'C', fontsize = 15);
axis([0, 0.5, 0, 100])

#savefig('\\temp\\fig10.png', dpi = 300)
```

3) c-program for printing the PHREEQC-2 input file.

```
#include <stdio.h>
#include <math.h>
#include <float.h>
#include <stdlib.h>

/* model Cs with f_free = 0.5, LK_NaSu = -0.7, Surf_A = 37 m2/g, only_counter TRUE, stagnant.
   with the ***3 sept 09*** log K's for Mg, Ca and Sr that give Pearson's distribution coeff's,
                            and sites and log K's for Cs.
   The tortuosity factors for filters are corrected relative to the sample */

/* subdivides the height of the column in nz layers. Set n_stagn = 0 to remove stagnant
   cell-numbering is 1) along z, 2) along x to ensure that calculations start from the
   source zone outward, i.e. if nz = 2:
   4 6 8 ...
   5 7 9 ...
 */
 static int find_timestep (double var1, double V4);
 static int find_mixf (void);
 static int print_mixf (void);
 static int print_transp (void);

 double Pi, r_int, r_ext, por, *por_cell, height, Dw, tort_n, *trt, total_time;
 double arc_length, A, A_out, Az, *dx, dz, dt, scale_f;
 double filter_dx, por_filter;
 double *V, *V_dl, *mixf, *mixf_z, *CECf, *iif;
 double V3;
 double LK_NaSu_, m_Su_, m_Su_ii, m_Su_fes, rho_b_eps, f_dl, surf_A, f_free, tDDL;
 double lgK_Cs_, lgK_Cs_ii, lgK_Cs_fes;
 double fr_stagn, mixf_stagn, k_kin;
 double var1, var2, var3, fitf, fitf2, fitf3, fitf3b, fitf4, lgK, Ki;
 int nx, n_stagn, nz, ncell, shifts, punch_fr, nf;
 int i, i1;
 FILE *f_out, *f_in;

int main(void)
{
/* radial diffusion cell, described in Van Loon et al., Environ. Sci. Technol. 2004, 38, 5721-5728
 */
 V = (double *) malloc(sizeof(double));     /* water volumes */
 V_dl = (double *) malloc(sizeof(double));  /* water in DDL */
 dx = (double *) malloc(sizeof(double));   /* cell-spacing */
 trt = (double *) malloc(sizeof(double));   /* cell-variable inverse tortuosity (multiplies Dw) */
 por_cell = (double *) malloc(sizeof(double));   /* cell-variable porosity */
 mixf = (double *) malloc(sizeof(double));  /* mixing in the radial (x) direction */
 mixf_z = (double *) malloc(sizeof(double));    /* mixing in the vertical (z) */
 CECf = (double *) malloc(sizeof(double));  /* cell dependent multiplicator for planar sites */
 iif = (double *) malloc(sizeof(double));   /* idem for ii and fes sites */

 nx = 11;                   /* radial cells in the model */
 nz = 1;                /* height discretization, horizontal layers */
 n_stagn = 1;           /* number of stagnant layers */
 fr_stagn = 0.1;        /* fraction of porewater with dead-end pores */
 fitf = 1.0;            /* multiplies CEC (not used here ) */
 fitf2 = 1.0;           /* multiplies Dp */
 fitf3 = 0.9;           /* sets CECf for mobile cells */
 fitf3b = 0.9;          /* sets iif idem */
 fitf4 = 0.1;           /* used in stagnant exchange factor */
 k_kin = 2e-11;         /* 4e-11, first order exchange constant for Cs */
 Ki = 0.424;            /* for linear sorption of I */
/* define surf_A and LK_NaSu_ for f_free = 0.25, which gives the apparent eps_an = 0.5
 */
 f_free = 0.5;
 surf_A = 5.245e5;   /* surface area of Su_, m2/(L total pore water) = 37 m2/g, cf Pearson, 2003 */
 LK_NaSu_ = -0.7;
 tDDL = (1 - f_free) * 1e-3 / surf_A;

 f_dl = 1 - f_free;     /* fraction of DDL water */
 por = 0.159;   /* total porosity */
 rho_b_eps = 2.7 * (1 - por) / por;  /* rho_b / eps, with rho_solid = 2.7 kg/L */
 nf = 1;            /* if > 0, filters are included, also number of
                       cells for the filter */

 /* for optimizing, read fit factors for CEC, Dw, etc....
```

```
 */
 f_in = fopen("cs_a1.txt", "r");
 fscanf(f_in, "%lf\n" "%lf\n" "%lf\n" "%lf\n" "%lf\n" "%lf\n" "%lf\n" "%d\n",
   &fitf, &fitf2, &fitf3, &fitf3b, &fitf4, &fr_stagn, &k_kin, &nx);
 fclose (f_in);

 if (fitf4 == 0) n_stagn = 0;
 if (fr_stagn == 0) n_stagn = 0;
 if (n_stagn == 0) fr_stagn = 0;

 /* define diffusion cell.
   sample: r_int = 6.58 mm, r_ext = 25.4 mm, height = 52 mm
   filter at 25.4 mm: filter_dx = 1.6 mm, por = 0.367
   filter at  6.58 mm, filter_dx = 1.8 mm, por = 0.418
 */
 r_int = 6.58e-3; r_ext = 0.0254; height = 0.052;
 ncell = (nx + 2 * nf) * nz;

 V3 = 1.014e-3 + 4.8e-6;        /* solution with tracers + dead volume, m3 */

 total_time = 100.0 * 24 * 3600;   /* s, is a subsample of the 940 days */
 trt = (double *) realloc(trt, (5 + ncell * (1 + n_stagn)) * sizeof(double));
 por_cell = (double *) realloc(por_cell, (5 + ncell * (1 + n_stagn)) * sizeof(double));
 dx = (double *) realloc(dx, (5 + ncell * (1 + n_stagn)) * sizeof(double));

 Dw = 2.12e-9;          /* m2/s for HTO at 23 0C, default Dw for calculating mixf's */
 if (n_stagn) {
   por = 0.161;
   tort_n = 0.949;      /* tort = 5.65 with 10% dead-end pores */
   f_dl = 0.50;
 } else {
   por = 0.159;
   tort_n = 0.987;      /* homogeneous, tort for optimized HTO = 6.15, por = 0.159 */
   f_dl = 0.495;
 }
/* redefine... */
 f_dl = 1 - f_free;     /* fraction of DDL water */

 i1 = 4;
 if (nf) {
   for (i = 4; i < 4 + nf * nz; i++) {
     trt[i] = 0.1 / 0.418 / pow(por, -tort_n) * 2.803 / fitf2;
     por_cell[i] = 0.418;
     dx[i] = 1.8e-3 / nf;
   }
   i1 = i;
   for (i = i1 + nx * (nz + n_stagn); i < 4 + nx * (nz + n_stagn) + 2 * nf * nz; i++) {
     trt[i] = 0.1 / 0.367 / pow(por, -tort_n) * 2.803 / fitf2;
     por_cell[i] = 0.367;
     dx[i] = 1.6e-3 / nf;
   }
 }
 for (i = i1; i < 4 + nf + nx; i++) {
   trt[i] = pow(por, tort_n);   /* the inverse tortuosity for HTO */
   por_cell[i] = por;
   dx[i] = (r_ext - r_int) / nx;
   if (n_stagn > 0) {
     trt[i + nx] = pow(por, tort_n);    /* the inverse tortuosity for HTO */
     por_cell[i + nx] = por;
     dx[i + nx] = (r_ext - r_int) / nx;
   }
 }
 if (nf) {
   r_int -= 1.8e-3;
   r_ext += 1.6e-3;
 }

 Pi = 2 * acos(0);
/* define cell volumes in m3, cylinder sections, filter at r_int + sample...
 */
 dz = height / nz;
 V = (double *) realloc(V, (5 + ncell * (1 + n_stagn)) * sizeof(double));
 V_dl = (double *) realloc(V_dl, (5 + ncell * (1 + n_stagn)) * sizeof(double));
 var2 = r_int;
 for (i = 0; i < ncell / nz - nf; i++) {
   var3 = dx[i + 4] + var2;
   var1 = var3 * var3 - var2 * var2;
```

```
   var1 *= dz * Pi;
   for (i1 = 0; i1 < nz; i1++) {
     V[i * nz + 4 + i1] = var1 * por_cell[i * nz + 4 + i1];
     if (i >= nf && i < nx + nf) V[i * nz + 4 + i1] *= (1 - fr_stagn);
/* this is for 1 stagnant layer only...
 */
     if (n_stagn > 0 && nz == 1 && i >= nf && i < nx + nf) {
       V[i + 4 + nx] = var1 * por_cell[i + 4 + nx] * fr_stagn;
     }
   }
   var2 = var3;
 }
/* filter at r_ext...
 */
 for (i = i + nx * n_stagn; i < ncell / nz + nx * n_stagn; i++) {
   var3 = dx[i + 4] + var2;
   var1 = var3 * var3 - var2 * var2;
   var1 *= dz * Pi;
   for (i1 = 0; i1 < nz; i1++) {
     V[i * nz + 4 + i1] = var1 * por_cell[i * nz + 4 + i1];
   }
   var2 = var3;
 }
 V[ncell + n_stagn * nx + 4] = 0.2e-3;

/* find timestep, mixf = Dw * trt * dt * A * por / dx / V = (1/3) / 2 at most
  for cell V[4] contacting the tracer solution...
 */
 var1 = 5.0 * 24.0 * 3600;      /* punch time, seconds */
 find_timestep (var1, V[4]);

/* define mixf's for a 1 L volume, actual volumes are given
    in SOLUTION; -water
 */
 mixf = (double *) realloc(mixf, (5 + ncell * (1 + n_stagn)) * sizeof(double));
 mixf_z = (double *) realloc(mixf_z, (5 + ncell * (1 + n_stagn)) * sizeof(double));
 find_mixf();

/* define factors for distributing CEC among the cells
 */
 CECf = (double *) realloc(CECf, (5 + ncell * (1 + n_stagn)) * sizeof(double));
 iif = (double *) realloc(iif, (5 + ncell * (1 + n_stagn)) * sizeof(double));
 if (n_stagn > 0) {
/* here for a model with dead-end pores...
 */
   for (i = nf; i < nx + nf; i++) {
     CECf[i + 4] = fitf3;
     iif[i + 4] = fitf3b;
   }
   for (i = nf; i < nx + nf; i++) {
     CECf[i + 4 + nx] = (1 - fitf3 * (1 - fr_stagn)) / fr_stagn;
     iif[i + 4 + nx] = (1 - fitf3b * (1 - fr_stagn)) / fr_stagn;
   }
 } else {
/* here for the homogeneous case, or for parallel layers...
 */
   for (i = nf; i < nx + nf; i++) {
     CECf[i + 4] = 1;
     iif[i + 4] = 1;
   }
 }
/* for (i = 1; i < ncell; i += nz) {
   CECf[i + 4] = 1.2;
   iif[i + 4] = 1.2;
 }
/* for (i = 2; i < ncell; i += nz) {
   CECf[i + 4] = 1;
   iif[i + 4] = 1;
 }
 */
/* A heterogeneous distribution of CEC retards the front,
   compensated with decreasing CEC...
 */

 var1 = Pi * (pow(r_ext - 1.6, 2) - pow(r_int + 1.8, 2)) * dz * por;

/* iif[9] = CECf[9] = 1.0 + 4 * (1 - CECf[4]) * (var1 - V[9]) / V[9];
```

```
 */
/* iif[9] = CECf[8] = 1.0 + 4 * (1 - CECf[4]) * (var1 - V[9] - V[14]) / V[9];
 iif[14] = CECf[14] = 1.0 + 4 * (1 - CECf[4]) * (var1 - V[9] - V[14]) / V[14];
 */

/* LK_NaSu_ is defined above, together with surf_A */
 if (n_stagn) {
   m_Su_ = 0.124;      /* mol/kg */
   m_Su_ii = 7.8892663E-04; m_Su_fes = 7.39755075E-05;  /* from isotherm optimization */
   lgK_Cs_ = 2.00;
   lgK_Cs_ii = 14.5997; lgK_Cs_fes = 17.14;
 } else {
   m_Su_ = 117.e-3;
   m_Su_ii = 0.786E-03; m_Su_fes = 0.07404e-3;
   lgK_Cs_ = 2.04;
   lgK_Cs_ii = 14.60; lgK_Cs_fes = 17.14;
 }
/* write the PHREEQC file...
 */
 f_out = fopen("cs1_4a1", "w");
 fprintf(f_out, "DATABASE c:\\dos\\p\\phreeqd.dat\n");
 fprintf(f_out, "SOLUTION_MASTER_SPECIES\n");
 fprintf(f_out, "#element       species alk     gfw_formula     element_gfw\n");
 fprintf(f_out, "Hto    Hto             0.0     1       1\n");
 fprintf(f_out, "Na_tr  Na_tr+          0.0     1       1\n");
 fprintf(f_out, "Cl_tr  Cl_tr-          0.0     1       1\n");
 fprintf(f_out, "Br_tr  Br_tr-          0.0     1       1\n");
 fprintf(f_out, "I_tr   I_tr-           0.0     1       1\n");
 fprintf(f_out, "Sr_tr  Sr_tr+2         0.0     1       1\n");
 fprintf(f_out, "Cs     Cs+             0.0     132.905         132.905\n");
 fprintf(f_out, "SOLUTION_SPECIES\n");
 fprintf(f_out, "Hto = Hto; log_k 0; -gamma 1e6 0; -dw %14.8e\n", 2.236e-9 * 1);
 fprintf(f_out, "Na_tr+ = Na_tr+; log_k 0; -gamma 4.0 0.075; -dw %14.8e\n", 1.33e-9 / trt[4 + nf] /
2.803 * fitf2);
 fprintf(f_out, "Cl_tr- = Cl_tr-; log_k 0; -gamma 3.5 0.015; -dw %14.8e\n", 2.03e-9 / trt[4 + nf] /
9.626 * fitf2);
 fprintf(f_out, "Br_tr- = Br_tr-; log_k 0; -gamma 3.6 0.015; -dw %14.8e\n", 2.01e-9 / trt[4 + nf] /
9.626 * fitf2);
 fprintf(f_out, "#Br_tr- + Na+ = NaBr_tr; log_k -1.3\n");
 fprintf(f_out, "I_tr- = I_tr-; log_k 0; -gamma 3.7 0.015; -dw %14.8e\n", 2.0e-9 / trt[4 + nf] /
9.626 * fitf2);
 fprintf(f_out, "Sr_tr+2 = Sr_tr+2; log_k 0; -gamma 5.26 0.121; -dw %14.8e\n", 0.993e-9 / trt[4 +
nf] / 2.803 * fitf2);
 fprintf(f_out, "Sr_tr+2 + SO4-2 = Sr_trSO4; log_k 2.29; delta_h 2.08 kcal; -dw %14.8e\n", 0.4e-9);
 fprintf(f_out, "Cs+ = Cs+; log_k 0; -gamma 3.5 0.015; -dw %14.8e\n", 2.07e-9 / trt[4 + nf] / 2.803
* fitf2);
 fprintf(f_out, "SURFACE_MASTER_SPECIES\n");
 fprintf(f_out, " Su_fes Su_fes-   # Frayed Edge Sites\n");
 fprintf(f_out, " Su_ii Su_ii-     # Type II sites of intermediate strength\n");
 fprintf(f_out, " Su_ Su_-         # Planar sites\n");
 fprintf(f_out, " Z Z         # for sorbing I, Br\n");
 fprintf(f_out, "SURFACE_SPECIES\n");
 fprintf(f_out, " Su_fes- = Su_fes-; log_k 0\n");
 fprintf(f_out, " Na+ + Su_fes- = NaSu_fes; log_k 10\n");
 fprintf(f_out, " Na_tr+ + Su_fes- = Na_trSu_fes; log_k 10\n");
 fprintf(f_out, " K+ + Su_fes- = KSu_fes; log_k 12.4\n");
 fprintf(f_out, " Cs+ + Su_fes- = CsSu_fes; log_k %14.8e\n", lgK_Cs_fes);
 fprintf(f_out, "\n");
 fprintf(f_out, " Su_ii- = Su_ii-; log_k 0\n");
 fprintf(f_out, " Na+ + Su_ii- = NaSu_ii; log_k 10\n");
 fprintf(f_out, " Na_tr+ + Su_ii- = Na_trSu_ii; log_k 10\n");
 fprintf(f_out, " K+ + Su_ii- = KSu_ii; log_k 12.1\n");
 fprintf(f_out, " Cs+ + Su_ii- = CsSu_ii; log_k %14.8e\n", lgK_Cs_ii);
 fprintf(f_out, "\n");
 fprintf(f_out, " Su_- = Su_-; log_k 0\n");
 fprintf(f_out, "Cs+ + Su_- = CsSu_; log_k %14.8e\n", LK_NaSu_ + lgK_Cs_);
 fprintf(f_out, "H+ + Su_- = HSu_; log_k %14.8e\n", LK_NaSu_ + 3 );
 fprintf(f_out, "Li+ + Su_- = LiSu_; log_k %14.8e\n", LK_NaSu_ - 0.1 );
 fprintf(f_out, "Na+ + Su_- = NaSu_; log_k %14.8e\n", LK_NaSu_ );
 fprintf(f_out, "Na_tr+ + Su_- = Na_trSu_; log_k %14.8e\n", LK_NaSu_ );
/* the K's give the Kd's as found with averaged Pearson log_K on X- */
 fprintf(f_out, "K+ + Su_- = KSu_; log_k %14.8e\n", 0.15);
 fprintf(f_out, "Mg+2 + 2Su_- = MgSu_2; log_k %14.8e\n", -0.56);
 fprintf(f_out, "Ca+2 + 2Su_- = CaSu_2; log_k %14.8e\n", -0.32);
 fprintf(f_out, "Sr+2 + 2Su_- = SrSu_2; log_k %14.8e\n", 0.21);
 fprintf(f_out, "Sr_tr+2 + 2Su_- = Sr_trSu_2; log_k %14.8e\n", 0.21);
 fprintf(f_out, " Z = Z; log_k 0\n");
```

```
 fprintf(f_out, " Z + I_tr- + Na+ = ZNaI_tr; log_k %14.8e\n", log10(1e-100 * Ki));
 fprintf(f_out, "# Z + Br_tr- + Na+ = ZNaBr_tr; log_k %14.8e\n", log10(1e100 * Ki));
 fprintf(f_out, "KNOBS; -iter 2000; -pe_step 5; -step 10; -diag true; -conv 1e-6\n");
 fprintf(f_out, "EXCHANGE_MASTER_SPECIES\n");
 fprintf(f_out, " Xkin Xkin-   # Frayed Edge Sites\n");
 fprintf(f_out, "EXCHANGE_SPECIES\n");
 fprintf(f_out, " Xkin- = Xkin-; log_k 0\n");
 fprintf(f_out, " K+ + Xkin- = KXkin; log_k 2.4\n");
 fprintf(f_out, " Cs+ + Xkin- = CsXkin; log_k 7.13  #17.13\n");
/* define Cs on X- ... */
 fprintf(f_out, " Cs+ + X- = CsX; log_k  %14.8e\n", lgK_Cs_);
 fprintf(f_out, "RATES\n");
#ifdef SKIP
 fprintf(f_out, " Sr_x\n");
 fprintf(f_out, " -start\n");
 fprintf(f_out, " 10 rate = %14.8e * (m - mol(\"Sr_trSu_2\") * tot(\"water\") * 1e11)\n", k_kin);
 fprintf(f_out, " 20 save rate * time\n");
 fprintf(f_out, " -end\n");
#endif
 fprintf(f_out, " Cs_xkin\n");
 fprintf(f_out, " -start # assume (0.2 * rho_b_eps) mol illite /L\n");
 fprintf(f_out, " 10 rate = %14.8e * (m - mol(\"CsXkin\") * tot(\"water\") * 1e11)\n", k_kin);
 fprintf(f_out, " 20 save rate * time\n");
 fprintf(f_out, " -end\n");
 if (k_kin > 0) {
   fprintf(f_out, "KINETICS %d-%d\n", 4 + nf, ncell - nf + n_stagn * nx + 3);
   fprintf(f_out, " Cs_xkin; -formula Cs 1 K -1; m 0\n");
 }
#ifdef SKIP
 /* kinetics for Sr... Note that log_k(Sr_trSu_2) must be decreased with -11.0
 */
 fprintf(f_out, "KINETICS %d-%d\n", 4 + nf, ncell - nf + n_stagn * nx + 3);
 fprintf(f_out, " Sr_x; -formula Sr_trCl2; m 0\n");
#endif
 fprintf(f_out, "END\n");

 fprintf(f_out, "\nSOLUTION 0-2; Na 1; Cl 1\n");
 fprintf(f_out, "END\n");

 fprintf(f_out, "\nSOLUTION 3; -water %14.8e\n", V3 * 1e3);
 fprintf(f_out, "pH 7.6; pe 14 O2(g) -1.0; temp 23\n");
   fprintf(f_out, "Na 240; K 1.61; Mg 16.9; Ca 25.8; Sr 0.505\n");
   fprintf(f_out, "Cl 300; S(6) 14.1; Fe(2) 0.0; Alkalinity 0.476\n");
 fprintf(f_out, "# Cl_tr 2.505e-2; Na_tr 1.87e-7 * 1e4; Sr_tr 2.71e-9 * 1e6; Hto 1.14e-6 * 1e3; Cs
1\n");
 fprintf(f_out, "# Br_tr 0.9684; I_tr 0.862\n");
 fprintf(f_out, "Cl_tr 0e-3; Na_tr 0e-3; Sr_tr 0; Hto 0e-3; Cs 1\n");
/* calculate alpha = eps + rho_b * Kd...
 */
 fprintf(f_out, "SURFACE 9999; -equil 3;  Su_ %14.8e %14.8e 1\n",
                 m_Su_ * rho_b_eps * V3 * 1e3 / (1 - f_dl), V3 * f_dl / (1 - f_dl) * 1e8);
 fprintf(f_out, " Su_ii %14.8e\n", m_Su_ii * rho_b_eps * V3 * 1e3 / (1 - f_dl));
 fprintf(f_out, " Su_fes %14.8e\n", m_Su_fes * rho_b_eps * V3 * 1e3 / (1 - f_dl));
 fprintf(f_out, " -donnan 1e-8 v 1; -only_co\n");
 fprintf(f_out, "USER_PRINT; -start;\n");
 fprintf(f_out, " 10 if tot(\"Sr_tr\") < 1e-20 then goto 50\n");
 fprintf(f_out, " 20 Kd = (sys(\"Sr_tr\") / (tot(\"Sr_tr\") * tot(\"water\") / %14.8e) - 1)\n", 1 -
f_dl);
 fprintf(f_out, " 30 print \' Kd_Sr = \', Kd\n");
 fprintf(f_out, " 40 print \' alpha = \', (1 + Kd) * %14.8e\n", por);
 fprintf(f_out, " 50 end; -end\n");
 fprintf(f_out, "END\n");

 for (i = 4; i < 4 + ncell + n_stagn * nx; i++) {
   if (i < 4 + nf || i >= 4 + ncell + n_stagn * nx - nf) {
     /* filters... */
     V[i] *= 1e3;
     V_dl[i] = 0;
     fprintf(f_out, "\nSOLUTION %d; -water %14.8e\n", i, V[i]);
     fprintf(f_out, "pH 7.6; pe 14 O2(g) -1.0; temp 23\n");
     fprintf(f_out, "Na 240; K 1.61; Mg 16.9; Ca 25.8; Sr 0.505\n");
     fprintf(f_out, "Cl 300; S(6) 14.1; Fe(2) 0.0; Alkalinity 0.476\n");
   } else {
     /* sample... */
     V_dl[i] = V[i] * 1e3 * f_dl;              /* DDL water, L */
     V[i] *= (1 - f_dl) * 1e3;                 /* free porewater, L */
     fprintf(f_out, "\nSOLUTION %d; -water %14.8e\n", i, V[i]);
```

```
    fprintf(f_out, "pH 7.6; pe 14 O2(g) -1.0; temp 23\n");
    fprintf(f_out, "Na 240; K 1.61; Mg 16.9; Ca 25.8; Sr 0.505\n");
    fprintf(f_out, "Cl 300; S(6) 14.1; Fe(2) 0.0; Alkalinity 0.476\n");
/* define surface, sp surf area = surf_A m2/L
 */
    fprintf(f_out, "SURFACE %d; -equil %d;  Su_ %14.8e %14.8e %14.8e\n", i, i,
/*                  mol_sites,                                        m2/L,   L  */
                    m_Su_ * CECf[i] * rho_b_eps * (V[i] + V_dl[i]), surf_A,
                    (V[i] + V_dl[i]));
    fprintf(f_out, " Su_ii %14.8e\n", m_Su_ii * iif[i] * rho_b_eps * (V[i] + V_dl[i]));
    fprintf(f_out, " Su_fes %14.8e\n", m_Su_fes * iif[i] * rho_b_eps * (V[i] + V_dl[i]));
    fprintf(f_out, " -donnan %14.8e v 1; -only_co\n", tDDL);
    fprintf(f_out, "# Z %14.8e 1e-6 1\n",
                     1e100 * rho_b_eps * (V[i] + V_dl[i]));
    if (k_kin > 0) {
/* With kinetics... Note that Xkin must be decreased with 10^-11.0
 */
      fprintf(f_out, "EXCHANGE %d; -equil %d;  Xkin %14.8e\n", i, i,
                     0.2 * iif[i] * rho_b_eps * (V[i] + V_dl[i]) * 1e-11);
    }
  }
 }
 fprintf(f_out, "\nSOLUTION %d; -water %14.8e\n", i, V[i] * 1e3);
 fprintf(f_out, "pH 7.6; pe 14 O2(g) -1.0; temp 23\n");
 fprintf(f_out, "Na 240; K 1.61; Mg 16.9; Ca 25.8; Sr 0.505\n");
 fprintf(f_out, "Cl 300; S(6) 14.1; Fe(2) 0.0; Alkalinity 0.476\n");
 fprintf(f_out, "END\n");

 print_mixf ();

/* define solids in which the tracers precipitate...
 */
 fprintf(f_out, "PHASES\n");
 fprintf(f_out, " A_cs\n");
 fprintf(f_out, " CsCl = Cs+ + Cl-; log_k -13\n");
 fprintf(f_out, " A_na\n");
 fprintf(f_out, " Na_trCl = Na_tr+ + Cl-; log_k -14\n");
 fprintf(f_out, " A_cl\n");
 fprintf(f_out, " NaCl_tr = Na+ + Cl_tr-; log_k -14\n");
 fprintf(f_out, " A_br\n");
 fprintf(f_out, " NaBr_tr = Na+ + Br_tr-; log_k -14\n");
 fprintf(f_out, " A_i\n");
 fprintf(f_out, " NaI_tr = Na+ + I_tr-; log_k -14\n");
 fprintf(f_out, " A_sr\n");
 fprintf(f_out, " Sr_trCl2 = Sr_tr+2 + 2Cl-; log_k -15\n");
 fprintf(f_out, " A_hto\n");
 fprintf(f_out, " Hto = Hto; log_k -15\n");
 fprintf(f_out, "EQUILIBRIUM_PHASES %d; A_cs 0 0; #A_hto 0 0; A_cl 0 0; A_na 0 0\n",
   4 + ncell + n_stagn * nx);
 fprintf(f_out, "END\n");

/* write transport and output... */
 fprintf(f_out, "PRINT; -reset false\n");
 fprintf(f_out, "SELECTED_OUTPUT;# -sel false; -user false\n");
 fprintf(f_out, " -file cs1_4a1.txt; -reset false; # -high_precision\n");
 fprintf(f_out, "USER_PUNCH; -head A_Cs/(1e-6mol) days\n");
 fprintf(f_out, "  10 if step_no = 0 then goto 100\n");
 fprintf(f_out, "  20 punch equi(\"A_cs\") * 1e6, total_time / (24 * 3600)\n");
 fprintf(f_out, "  100 end\n");
 fprintf(f_out, "USER_GRAPH; -head days J_Cs/(mol/m2/s) A_cs/mol m_Cs_inlet\n");
 fprintf(f_out, " -connect t\n");
 fprintf(f_out, " -plot_conc t\n");
 fprintf(f_out, " -plot_csv_file \\werk2\\nagra\\cs\\j_data.txt\n");
 fprintf(f_out, " -axis_scale y_axis 0 2e-9\n");
 fprintf(f_out, "# -axis_scale y_axis 0 2e-9\n");
 fprintf(f_out, "# -axis_scale x_axis 0 1000\n");
 fprintf(f_out, " -start\n");
 fprintf(f_out, "  10 graph_x total_time / (24 * 3600)\n");
 fprintf(f_out, "  12 if cell_no = 3 then goto 100\n");
 fprintf(f_out, "  20 A_hto = equi(\"A_hto\") * 1e-3 \n");
 fprintf(f_out, "  30 A_na = equi(\"A_na\") * 1e0\n");
 fprintf(f_out, "  32 A_sr = equi(\"A_sr\") * 1e7\n");
 fprintf(f_out, "  34 A_cs = equi(\"A_cs\") \n");
 fprintf(f_out, "  40 J_hto = (A_hto - get(1)) * %14.8e\n", 1.0 / (dt * punch_fr) / (A_out * nz));
 fprintf(f_out, "  50 J_na = (A_na - get(2)) * %14.8e\n", 1.0 / (dt * punch_fr) / (A_out * nz));
 fprintf(f_out, "  52 J_sr = (A_sr - get(3)) * %14.8e\n", 1 / (dt * punch_fr) / (A_out * nz));
 fprintf(f_out, "  54 J_cs = (A_cs - get(4)) * %14.8e\n", 1.0 / (dt * punch_fr) / (A_out * nz));
```

```
 fprintf(f_out, "  60 graph_y J_cs\n");
 fprintf(f_out, "  62 graph_sy A_cs\n");
 fprintf(f_out, "  80 put(A_hto, 1)\n");
 fprintf(f_out, "  90 put(A_na, 2)\n");
 fprintf(f_out, "  92 put(A_sr, 3)\n");
 fprintf(f_out, "  94 put(A_cs, 4)\n");
 fprintf(f_out, "  96 goto 150\n");
 fprintf(f_out, "  100 graph_y tot(\"Cs\")\n");
 fprintf(f_out, "  150 end\n");
 fprintf(f_out, " -end\n");

 fprintf(f_out, "TRANSPORT\n");
 fprintf(f_out, " -shifts %d\n", shifts);
 fprintf(f_out, " -war true; -flow diff; -cells 1; -bcon 1 2; -stag %d\n",
   ncell + n_stagn * nx + 2);
 fprintf(f_out, " -time %14.8e\n", dt);
 fprintf(f_out, " -multi_D true %14.8e %14.8e 0.0 %14.8e\n", Dw, por, tort_n);
 fprintf(f_out, "# -interlayer_D true 0.04 0.0 475\n");
 fprintf(f_out, " -punch_fr %d; -punch_c %d\n", punch_fr, 4 + ncell + n_stagn * nx);
 fprintf(f_out, " -print_fr %d\n", shifts);
 fprintf(f_out, "END\n");

/* correct volume of tracer solution for sampling ...
 */
 fprintf(f_out, "\n#PRINT; -sel false\n");
 fprintf(f_out, "MIX 3\n");
 fprintf(f_out, "3 0.994\n");
 fprintf(f_out, "SAVE SOLUTION 3 # days 100 - 200\n");
 fprintf(f_out, "END\n");
 total_time = 100.0 * 24 * 3600;   /* 200 days */
 find_timestep (5.0 * 24 * 3600, (V[4] + V_dl[4]) * 1e-3);
 find_mixf (); print_mixf (); print_transp ();

 fprintf(f_out, "\n#PRINT; -sel false\n");
 fprintf(f_out, "MIX 3\n");
 fprintf(f_out, "3 0.994\n");
 fprintf(f_out, "SAVE SOLUTION 3 # days 200 - 300\n");
 fprintf(f_out, "END\n");
 total_time = 100.0 * 24 * 3600;   /* 300 days */
 find_timestep (5.0 * 24 * 3600, (V[4] + V_dl[4]) * 1e-3);
 find_mixf (); print_mixf (); print_transp ();

 fprintf(f_out, "\n#PRINT; -sel false\n");
 fprintf(f_out, "MIX 3\n");
 fprintf(f_out, "3 0.9945\n");
 fprintf(f_out, "SAVE SOLUTION 3 # days 300 - 400\n");
 fprintf(f_out, "END\n");
 total_time = 100.0 * 24 * 3600;   /* 400 days */
 find_timestep (5.0 * 24 * 3600, (V[4] + V_dl[4]) * 1e-3);
 find_mixf (); print_mixf (); print_transp ();

 fprintf(f_out, "\n#PRINT; -sel false\n");
 fprintf(f_out, "MIX 3\n");
 fprintf(f_out, "3 0.9943\n");
 fprintf(f_out, "SAVE SOLUTION 3 # days 400 - 500\n");
 fprintf(f_out, "END\n");
 total_time = 100.0 * 24 * 3600;   /* 500 days */
 find_timestep (5.0 * 24 * 3600, (V[4] + V_dl[4]) * 1e-3);
 find_mixf (); print_mixf (); print_transp ();

 fprintf(f_out, "\n#PRINT; -sel false\n");
 fprintf(f_out, "MIX 3\n");
 fprintf(f_out, "3 0.994\n");
 fprintf(f_out, "SAVE SOLUTION 3 # days 500 - 600\n");
 fprintf(f_out, "END\n");
 total_time = 100.0 * 24 * 3600;   /* 600 days */
 find_timestep (5.0 * 24 * 3600, (V[4] + V_dl[4]) * 1e-3);
 find_mixf (); print_mixf (); print_transp ();

 fprintf(f_out, "\n#PRINT; -sel false\n");
 fprintf(f_out, "MIX 3\n");
 fprintf(f_out, "3 0.994\n");
 fprintf(f_out, "SAVE SOLUTION 3 # days 600 - 700\n");
 fprintf(f_out, "END\n");
 total_time = 100.0 * 24 * 3600;   /* 700 days */
 find_timestep (5.0 * 24 * 3600, (V[4] + V_dl[4]) * 1e-3);
 find_mixf (); print_mixf (); print_transp ();
```

```
 fprintf(f_out, "\n#PRINT; -sel false\n");
 fprintf(f_out, "MIX 3\n");
 fprintf(f_out, "3 0.995\n");
 fprintf(f_out, "SAVE SOLUTION 3 # days 700 - 800\n");
 fprintf(f_out, "END\n");
 total_time = 100.0 * 24 * 3600;   /* 800 days */
 find_timestep (5.0 * 24 * 3600, (V[4] + V_dl[4]) * 1e-3);
 find_mixf (); print_mixf (); print_transp ();

 fprintf(f_out, "\n#PRINT; -sel false\n");
 fprintf(f_out, "MIX 3\n");
 fprintf(f_out, "3 0.993\n");
 fprintf(f_out, "SAVE SOLUTION 3 # days 800 - 940\n");
 fprintf(f_out, "END\n");
 total_time = 140.0 * 24 * 3600;   /* 940 days */
 find_timestep (5.0 * 24 * 3600, (V[4] + V_dl[4]) * 1e-3);
 find_mixf (); print_mixf (); print_transp ();

 fclose(f_out);
 free (V); free (dx); free (trt); free (por_cell); free (V_dl); free (mixf);
 free (mixf_z); free (CECf); free (iif);
 return 0;
}

int find_timestep (double var1, double V4)
{
 A = 2.0 * Pi * r_int * dz;
 dt = dx[4] * V4 / (Dw * (trt[4] / 2.803 * fitf2) * A * por_cell[4]) / 15;
  if (dt >= var1) {
    punch_fr = 1;
    dt = var1;
 } else {
    punch_fr = (int) ceil(var1 / dt);
    dt = var1 / punch_fr;
 }
 shifts = (int) ceil(total_time / dt);
 if (shifts * dt > total_time + dt / 2) shifts -= 1;
 return 0;
}

int find_mixf (void)
{
/* calculate the flux F = -2 (g_1 * g_2) Dw / (g_2 * x_1 + g_1 * x_2) * (c_2 - c_1)
   multiply with dt * A / (V = 1e-3 m3).  (Actual volumes are given with SOLUTION; -water)
   g_1 = por_1 * trt_1, g_2 = por_2 * trt_2, x_1 = Delta(x_1), etc.
 */
 double g1, g2, x1, x2;

 A = 2.0 * Pi * r_int * dz;
 mixf[3] = Dw * trt[4] * dt * A * por_cell[4] * 2 / dx[4] / 1e-3;
 if (!nf) mixf[3] *= (1 - fr_stagn);
 var2 = r_int;
/* filter at r_int + sample...
 */
 for (i = 0; i < ncell / nz - nf; i++) {
   if (!nf && i == ncell / nz -1) continue;
   var3 = dx[i * nz + 4] + var2;
   A = 2 * Pi * var3 * dz;
   Az = Pi * (var3 * var3 - var2 * var2);
   for (i1 = 0; i1 < nz; i1++) {
     g1 = por_cell[i * nz + 4 + i1] * trt[i * nz + 4 + i1];
     x1 = dx[i * nz + 4 + i1];
     if (n_stagn > 0 && i == nx + nf - 1) {
       g2 = por_cell[i * nz + 5 + n_stagn * nx + i1] * trt[i * nz + 5 + n_stagn * nx + i1];
       x2 = dx[i * nz + 5 + n_stagn * nx + i1];
     } else {
       g2 = por_cell[i * nz + 5 + i1] * trt[i * nz + 5 + i1];
       x2 = dx[i * nz + 5 + i1];
/* the vertical diffusion rate is 3* smaller than horizontal...
 */
       mixf_z[i * nz + 4 + i1] = Dw * trt[i * nz + 4 + i1] / 3;
       mixf_z[i * nz + 4 + i1] *= (dt * Az * por_cell[i * nz + 4 + i1] / dz / 1e-3);
     }
     mixf[i * nz + 4 + i1] = 2 * g1 * g2 / (g2 * x1 + g1 * x2) * Dw * dt * A / 1e-3;
     if (i >= nf && i < nx + nf) mixf[i * nz + 4 + i1] *= (1 - fr_stagn);
     if (n_stagn > 0 && nz == 1 && i >= nf && i < nx + nf) {
```

```
/* the vertical diffusion rate is fitf4* (or 3*) smaller than horizontal...
 */
      mixf_z[i * nz + 4 + i1] = Dw * trt[i * nz + 4 + i1] / fitf4;
      mixf_z[i * nz + 4 + i1] *= (dt * Az * por_cell[i * nz + 4 + i1] / dz / 1e-3);
    }
  }
  var2 = var3;
 }
/* filter at r_ext...
 */
 for (i = ncell / nz - nf + nx * n_stagn; i < ncell / nz + nx * n_stagn; i++) {
  var3 = dx[i * nz + 4] + var2;
  A = 2 * Pi * var3 * dz;
  Az = Pi * (var3 * var3 - var2 * var2);
  for (i1 = 0; i1 < nz; i1++) {
    mixf[i * nz + 4 + i1] = Dw * trt[i * nz + 4 + i1] * dt * A * por_cell[i * nz + 4 + i1] /
        dx[i * nz + 4 + i1] / 1e-3;
    mixf_z[i * nz + 4 + i1] = Dw * trt[i * nz + 4 + i1] / 3 * dt * Az * por_cell[i * nz + 4 + i1] /
        dz / 1e-3;
  }
  var2 = var3;
 }
 A_out = A = 2 * Pi * r_ext * dz;
 var1 = Dw * trt[3 + ncell + n_stagn * nx] * dt * A * por_cell[3 + ncell + n_stagn * nx] * 2;
 var1 /= (dx[3 + ncell + n_stagn * nx] * 1e-3);
 if (!nf) var1 *= (1 - fr_stagn);
 for (i = 0; i < nz; i++) {
  mixf[i + 4 + ncell + n_stagn * nx - nz] = var1;
 }
 return 0;
}

int print_mixf (void)
{
 /* mixing with the tracer solution...
 */
 fprintf(f_out, "MIX 3\n");
 for (i = 4; i <= 3 + nz; i++) {
  fprintf(f_out, " %d %14.8e\n", i, mixf[3]);
 }
/* filter at r_int + sample...
 */
 for (i = 0; i < ncell / nz - nf; i++) {
  for (i1 = 0; i1 < nz; i1++) {
    if (n_stagn && i == ncell / nz - nf - 1) {
      fprintf(f_out, "MIX %d; %d %14.8e\n", i * nz + 4 + i1, i * nz + 5 + i1 + nx * n_stagn,
        mixf[i * nz + 4 + i1]);
    } else {
      fprintf(f_out, "MIX %d; %d %14.8e\n", i * nz + 4 + i1, i * nz + 5 + i1,
        mixf[i * nz + 4 + i1]);
    }
    if (i1 < nz - 1) {
      fprintf(f_out, "%d %14.8e\n", i + i1 + 1, mixf_z[i * nz + 4 + i1]);
    }
  }
  if (n_stagn > 0 && nz == 1 && i >= nf && i < ncell - nf) {
    for (i1 = 0; i1 < n_stagn; i1++) {
      fprintf(f_out, "%d %14.8e\n", i + 4 + nx * n_stagn, mixf_z[i * nz + 4 + i1]);
    }
  }
 }
/* filter at r_ext...
 */
 for (i = i + nx * n_stagn; i < ncell / nz + nx * n_stagn; i++) {
  for (i1 = 0; i1 < nz; i1++) {
    fprintf(f_out, "MIX %d; %d %14.8e\n", i * nz + 4 + i1, i * nz + 5 + i1,
      mixf[i * nz + 4 + i1]);
    if (!nf && n_stagn > 0 && nz == 1) {
      fprintf(f_out, "%d %14.8e\n", i + nx, mixf_z[i]);
    }
  }
 }
 fprintf(f_out, "END\n");
 return 0;
}
int print_transp (void)
{
```

```
 fprintf(f_out, "\n#PRINT; -sel true\n");
 fprintf(f_out, "TRANSPORT\n");
 fprintf(f_out, " -shifts %d\n", shifts);
 fprintf(f_out, " -time %15.9e\n", dt);
 fprintf(f_out, " -punch_fr %d; -punch_c %d\n", punch_fr, 4 + ncell + n_stagn * nx);
 fprintf(f_out, " -print_fr %d\n", shifts);
 fprintf(f_out, "END\n");

 return 0;
}
```